Title: Vaccine-enhanced competition permits rational bacterial strain replacement in the gut

Authors: Verena Lentsch[1,2], Aurore Woller[3,4], Andrea Rocker[5], Selma Aslani[1], Claudia Moresi[1], Niina Ruoho[1], Louise Larsson[1], Stefan A. Fattinger[6,7], Nicolas Wenner[5], Elisa Cappio Barazzone[1], Wolf-Dietrich Hardt[6], Claude Loverdo[3], Médéric Diard[5,8*], Emma Slack[1,8,9*]

Affiliations:

1. Institute for Food, Nutrition and Health, ETH Zurich; Zurich, Switzerland

2. Medical Research Council (MRC) Translational Immunology Discovery Unit, MRC Weatherall Institute of Molecular Medicine (WIMM), John Radcliffe Hospital, University of Oxford, UK

3. Sorbonne Université, CNRS, Institut de Biologie Paris-Seine (IBPS), Laboratoire Jean Perrin (LJP); Paris, France

4. Unité de Chronobiologie théorique, Faculté des Sciences, Université Libre de Bruxelles (ULB); Brussels, Belgium

5. Biozentrum, University of Basel; Basel, Switzerland

6. Institute for Microbiology, Department of Biology, ETH Zurich; Zurich, Switzerland

7. Science for Life Laboratory, Department of Medical Biochemistry and Microbiology, Uppsala University; Uppsala, Sweden

8. Basel Research Centre for Child Health, Basel, Switzerland

9. Sir William Dunn School of Pathology, University of Oxford, UK

* Correspondence: emma.slack@hest.ethz.ch; mederic.diard@unibas.ch

Abstract: Colonization of the intestinal lumen precedes invasive infection for a wide range of enteropathogenic and opportunistic pathogenic bacteria. Here we show that combining oral vaccination with engineered or selected niche-competitor strains permits pathogen exclusion and strain replacement in the mouse gut lumen. This approach can be applied both prophylactically to prevent invasion of non-typhoidal *Salmonella* strains, or therapeutically to displace an established *Escherichia coli.* Both intact adaptive immunity and metabolic niche competition are necessary for efficient vaccine-enhanced competition. Our findings imply that mucosal antibodies have evolved to work in the context of gut microbial ecology, by influencing the outcome of competition. This has broad implications for the elimination of pathogenic and antibiotic-resistant bacterial reservoirs, and for rational microbiota engineering.

One sentence summary: Combining oral vaccination with a bacterial niche competitor allows complete replacement of wildtype *Salmonella* or *Escherichia coli* with non-pathogenic strains in the gut lumen.

Keywords: Oral vaccine, niche competition, microbiota, IgA, Salmonella, probiotic

Main Text:

Introduction

Drug-resistant infections with *Escherichia coli* (*E. coli*) and *Salmonella* spp. are increasing (*1*). Both species typically colonize the gut before initiating disease and can be carried asymptomatically in the gut lumen. There is a pressing need for control and prevention strategies that are independent of antibiotics, and which target not only disease but also gut pathogen reservoirs.

Most current vaccines focus on clearing infection from tissues, relying on serum antibodies and cellular immunity. However, protection from colonization of the gut lumen, topologically outside of the body, is fundamentally different. Invasion into this densely populated microbial ecosystem is a crucial step in enteropathogenic bacterial infections(*2, 3*). Correspondingly, the microbiota plays a role in recovering homeostasis and excluding colonizing opportunistic pathogens (*4, 5*). For example, fecal microbiota transplantation can be curative in recurrent *Clostridioides difficile* infections (*6*) and dietary shifts or antibiotic treatment break colonization resistance, permitting *Salmonella* infection (*3*). Consequently, protective intestinal immune mechanisms have evolved to work in the context of gut microbial ecology.

Whole-cell inactivated oral vaccines induce high-affinity T cell-dependent IgA responses against the *Salmonella enterica* subspecies *enterica* serovar Typhimurium (*S.*Tm) and *E. coli* surface, including the O-antigens of lipopolysaccharide (*7, 8*). This IgA response aggregates *S.*Tm in the gut lumen via enchained growth, increasing bacterial clearance due to rapid flushing of aggregates, and exerting a selective pressure (*7, 9*). Consequently, oral vaccination can alter the outcome of competition between O-antigen variants of *Salmonella* (*10*). Generalizing this concept, we expect high-affinity IgA to generate a fitness disadvantage for any targeted strain. Combining oral vaccination with oral supplementation of a live bacterial

niche competitor could therefore drive competitive exclusion of the pathogen. An ideal niche competitor would be a non-pathogenic strain with complete metabolic niche overlap, a faster growth-rate, and an absence of surface antigen cross-reactivity to the pathogen of interest. We here define the combination of a whole-cell inactivated oral vaccine with a live niche competitor as "vaccine-enhanced competition".

To explore the quantitative limits of vaccine-enhanced competition, we generated a model. This is based on exponential growth of wildtype *Salmonella,* a competitor strain and the microbiota (modelled as a single entity) in the presence of finite shared and private niches, and clearance due to flow and death. Kinetic parameters were estimated from *in vivo* competition assays, combined with direct quantification of bacterial generation numbers using the unstable plasmid pAM34 (*11*) (Supplementary Model). Finite niches were defined to be (i) available to the microbiota only, (ii) available to *Salmonella* and its competitor only, or (iii) competitively used by both *Salmonella* and the microbiota (see Supplementary Model Text). The rate of elimination of the target is expected to be related to (i) the magnitude of IgA-driven increase in clearance rate of the target and (ii) the extent of metabolic competition between the competitor and target strains, which suppresses the available niche for the pathogen (Supplementary model text). The model predicts clearance of virulent *Salmonella* within a few days if a typical IgA response is combined with a fast-replicating competitor. Neither IgA alone, nor competitor alone led to complete clearance. The model predicts complete robustness to the timing of competitor introduction, if some competitor bacterium is present at the time of challenge.

Using these timings as a guide, we explored vaccine-enhanced competition in the context of two *in vivo* models. Firstly, we applied vaccine-enhanced competition to prevent disease and eliminate colonization in the murine model of non-typhoidal Salmonellosis in resistant (Nramp1$^{+/+}$) mice (*12, 13*). Secondly, we demonstrated that vaccine-enhanced competition

66 can be applied therapeutically to eliminate *E. coli* from the gut lumen of C57BL/6 mice.
67 Vaccine-enhanced competition has broad potential to manipulate enterobacteriaceal
68 colonization and disease.

Salmonella-based niche competitors enhance vaccine protection

As a proof-of-concept, a niche-competitor with complete metabolic niche overlap was constructed by engineering the pathogen itself i.e., *S.*Tm SL1344. To improve competitive fitness and abolish virulence, we deleted the master regulator of *Salmonella* Pathogenicity Island 1 (SPI-1) genes, *hilD,* and the *Salmonella* Pathogenicity Island 2 (SPI-2) component *ssaV* (*14, 15*). Antibody cross-reactivity was reduced by inactivating the abequose O-acetylase *oafA (16),* converting the wildtype serovar O:4[5],12 to O:4,12 serovar *S.*Tm^{Comp} (**fig. S1**). It should be noted that the O-antigen densely carpets the surface of *Salmonella*, and O-antigen modification alone is therefore sufficient to dramatically decrease live-cell recognition by antibodies specific for the unmodified O-antigen (*10*).

We first tested vaccine-enhanced competition based on oral vaccination against the wildtype *S.*Tm, combined with pre-colonization with *S.*Tm^{Comp} at 3 days or 19 days prior to challenge in the streptomycin non-typhoidal Salmonellosis model (*12*) (**Fig. 1A, fig. S2**). Antibody titres at endpoint were not altered by the presence of *S.*Tm^{Comp} (**Fig. 1B).** In control mice, *S.*Tm^{WT} robustly colonized the gut lumen to day 10 post-infection (**Fig 1C+D, fig. S2)**. Niche competitor (*S.*Tm^{Comp}) or oral vaccination alone mildly suppressed colonization (**Fig. 1C+D, fig. S2)**. In mice that were both vaccinated and colonized with *S.*Tm^{Comp}, *S.*Tm^{WT} initially colonized poorly (**Fig. 1D, fig. S2**) and was rapidly cleared. *S.*Tm^{WT} was undetectable in the cecum content in 7 of 13 mice in this group at day 10 of infection (**Fig. 1C+D, fig. S2**), and was suppressed more than 100’000-fold in the remaining animals. As *S.*Tm^{Comp} persists at low levels for several weeks in our SPF mouse colony (**fig. S1**), the time of pre-colonization with *S.*Tm^{Comp} did not significantly influence clearance efficacy (**fig. S2, fig. S3**). This is practically important as it indicates that a niche competitor can be fed considerably before an infection occurs. This highlights the need for rigorous safety testing, as these organisms need to colonize the gut long-term or to be delivered frequently.

Wherever *S.*Tm^{WT} was rapidly eliminated from the gut lumen, systemic sites were also sterile (**Fig. 1E+F, fig. S2).** Pathology, as measured longitudinally by fecal Lipocalin-2 (LCN2) and at endpoint by histopathology (**Fig. 1G-I)** mirrored intestinal colonization. Pathology was prevented by the vaccine-enhanced competition regimen, but only partially prevented by each intervention alone.

To further corroborate our findings of sterilizing immunity, we performed fecal microbiota transplants (FMT) from infected vaccine-enhanced competition-treated mice at day 9 into naïve streptomycin pretreated mice (**Fig. 1A**). Transfer of 1 to 10 CFUs is sufficient to cause full-blown disease in this model (*15, 17*). Despite the high-dose fecal transfer, only one animal of eight showed transmission of *S.*Tm^{WT} (**Fig. 1J+K**). Intriguingly, this donor did not have the highest fecal *S.*Tm^{WT} counts at the time of transfer, but the lowest competitor:wildtype ratio of all donors (40-fold excess, compared to over 1000-fold excess). This suggests an additional benefit of the approach: a competitor can prevent transmission even in cases where sterilizing immunity in the gut lumen is incomplete. In contrast, all mice receiving feces from the untreated control group of *S.*Tm-infected mice became infected (**Fig. 1J+K**). Therefore vaccine-enhanced competition permitted clearance of high-dose *S.*Tm^{WT} challenge from the gut and prevention of invasion into all examined sites. This also largely prevented transmission to naïve hosts, providing herd immunity.

Metabolic niche overlap is necessary for vaccine-enhanced competition

To investigate whether vaccine-mediated clearance from the gut lumen required complete metabolic niche overlap, we compared the functionality of *S.*Tm^{Comp} to a galactitol-utilization mutant *S.*Tm$^{Comp\ \Delta gatABC}$ (**Fig. 2A**) (*18, 19*). Lack of overlap for a single sugar (galactitol) in the competitor resulted in significantly slower competitive exclusion of *S.*Tm^{WT} in vaccinated mice, as compared to a full niche overlap (**Fig. 2B**). The mechanism therefore requires metabolic niche overlap.

We next investigated the ability of a more distantly related mouse commensal B2 *E. coli* 8178 (*Ec*^{8178}) to act as a niche competitor against *S.*Tm. This strain has a partial niche overlap with *S.*Tm *in vivo (20, 21)*. A benefit of using a more distantly related probiotic is that this *E. coli* produces a completely unrelated O-antigen structure, allowing us to use the "evolutionary trap" version of our *S.*Tm vaccine (*10*) (**Fig. 3A**) i.e., a version of the vaccine covering all common *S.*Tm O-antigen variations. Colonization with *Ec*^{8178} did not induce detectable *Ec*^{8178}-binding intestinal IgA nor serum IgG (**fig. S4**). Vaccine-enhanced competition based on combining the *S.*Tm^{WT}-vaccination with *Ec*^{8178} could decrease initial *S.*Tm^{WT} expansion about 1000-fold and completely prevented gut inflammation (**Fig. 3B-H**) (*7, 22*).

These experiments were then repeated using a completely unrelated probiotic strain (*Lactobacillus casei*), that has minimal niche overlap with *Salmonella (23).* Despite robust colonization, *L. casei* had no significant effect on vaccine-mediated protection (**fig. S5**).

A final aspect of niche competition tested is whether a more intact microbiome may contribute to niche competition. High-fat diet feeding induces mild and transient microbiota disruption (*21*). In this model, oral vaccination alone and niche-competitor alone were effective in preventing *Salmonella* colonization. However, vaccine-enhanced competition performed slightly better in preventing disease, suggesting that combining oral vaccination and niche competition has benefits also in the presence of natural competitors (**fig. S6**). In the murine typhoid model, mice are orally infected with a high dose of *Salmonella* without pretreatment or pre-existing damage to the microbiota (*13*). Vaccine-enhanced competition also provides robust protection from colonization and gut inflammation in this model. Of note, as the high infection dose permits immediate invasion of *Salmonella* into Peyer's patches, protection of systemic sites was weak in this model (**fig. S7**) (*7, 24-26*).

Vaccine-enhanced competition can displace an *E. coli* strain from the gut microbiota

To discover whether vaccine-enhanced competition can eliminate a strain already present in the microbiota we used the non-encapsulated commensal *E. coli* strain HS as a target (*27*). These experiments were performed in C57BL/6 mice carrying a low-complexity microbiota that permits continuous *E. coli* colonization at up to 10^8 CFU/g feces without antibiotic pretreatment (*28*). After pre-colonization with *E. coli* HS, mice were fed oral vaccine on days 3, 13 and 20 and the niche-competitor cocktail on days 10 and 17. *E. coli* HS and niche competitor levels were monitored in feces until day 23 (**Fig. 4A**). Whole-cell inactivated oral vaccines for *E. coli* HS induced an IgA response against the surface of live *E. coli* HS, but not against the three *E. coli* strains making up the niche-competitor probiotic (**Fig. 4B**). Vaccine-enhanced competition resulted in complete displacement of the targeted *E. coli* strain in 50% of the treated animals, with strongly suppressed colonization seen in the remaining animals (**Fig. 4C+D**). Each treatment alone had only a very mild effect on *E. coli* HS colonization levels (**Fig. 4C+D**).

Therefore, the concept of oral vaccine-driven strain replacement is generalizable to non-encapsulated *E. coli* and can eradicate a bacterium already present in the gut microbiota.

Vaccine-enhanced competition requires intact adaptive immune system

Finally, as immune stimulation could potentially induce antibody-independent effects contributing to pathogen clearance (*29*), we tested the role of adaptive immunity in vaccine-enhanced competition. As genetically immunodeficient lines were not easily available, we used antibodies to depleted more than 90% of all $CD4^+$ T cells and B cells from the spleen, mesenteric lymph nodes and blood of treated mice (**Fig. 5A+B, fig. S8**). $CD4^+$ T cell and B cells depletion during the vaccination period strongly suppressed induction of vaccine-specific IgA in both SPF 129SJL mice and gnotobiotic C57BL/6 mice (**Fig. 5C, fig. S8**). In the therapeutic clearance of *E. coli,* suppression of T-dependent antibody responses completely prevented *E. coli* HS elimination, while isotype-treated mice robustly cleared

E. coli HS. This is consistent with a major contribution of vaccine-induced adaptive immunity (**Fig. 5D+E**). In prevention of *Salmonella* using Ec^{8178} as a competitor, only the isotype-control-treated mice receiving the vaccination-enhanced protection treatment remained healthy throughout the experiment, with no bloom of *Salmonella* and effective prevention of systemic spread (**fig. S8**), again confirming the role of vaccine-induced adaptive immunity. Conversely, depleting $CD4^+$ and $CD8^+$ T cells only after vaccination, i.e. after induction of a T cell-dependent antibody responses, had no impact on vaccine-enhanced competition (**fig. S9**). As the only adaptive immune component present in non-inflamed gut are secretory antibodies, these findings are consistent with a role of T-dependent IgA in vaccine-enhanced competition.

Our high-dose inactivated oral vaccines are not potent inducers of effector T cell responses, in contrast to live-attenuated vaccines (*24*). Correspondingly, live-attenuated vaccines are poor at preventing gut colonization but do generate T cell-dependent protection of deep tissues (**fig. S9**). This highlights a dichotomy in protective mechanisms between the gut lumen and systemic sites and between vaccine-enhanced competition and live-attenuated *Salmonella* vaccines.

Discussion

The concept that gut microbes contribute to prevention of pathogen colonization is well accepted (*2, 3, 30, 31*). We know secretory IgA increases the clearance rate of intestinal *Salmonella* and *E. coli* via enchained growth (*7*), and that this exerts selective pressure on IgA-targeted bacteria (*10*). Here, we show that these processes work best together. This represents a fundamental shift in approach to designing vaccines for enteric bacteria. Published nutrient blocking and rationally designed microbiome engineering approaches can

supress *Salmonella* loads to around 10^5 CFU/g feces (*32, 33*), while our combined approach can generate more than a 10^9-fold reduction in colonization, down to undetectable levels.

Vaccine-enhanced competition requires both rational oral vaccine design and optimal niche competitor selection. Earlier work on evolutionary trap vaccines provided a starting point for oral vaccine design targeting the O-antigen of non-encapsulated *Enterobacteriaceae* (*10*). Here, we explored two ends of the spectrum for niche competitor selection/design, first by rationally modifying the target strain itself to generate a "perfect" competitor and second by testing commensal *E. coli* strains and a distantly related *Lactobacillus* strain (*21, 27*). There has been considerable progress in the genomic prediction of community function and metabolic niche overlap(*34*), recently defined as nutrient blocking (*32*), indicating improved approaches are likely to involve designed niche competitor consortia.

We can imagine several scenarios where this type of prophylaxis could be relevant. Prevention of enteropathogenic bacterial infections during travel could be achieved by vaccine-enhanced competition, given shortly before and potentially during travel. Orally administered vaccines and probiotics are ideal for self-administration. Additionally, we have shown that we can replace a strain already present in the gut, which allows elimination of opportunistic pathogen reservoirs, for example in patients scheduled for high-risk interventions (*35, 36*). This could be game-changing in preventing invasive, and increasingly multi-drug-resistant disease in vulnerable human patients. Another interesting hypothesis is that IgA-mediated strain replacement may occur frequently without our intervention, i.e. is an evolved function of secretory IgA. This is consistent with observations of instability of *E. coli* at the strain level, but not the species level, over time in healthy volunteers (*37*).

Our observations may also explain some controversies in the existing *Salmonella* literature. For example, the extent of protection from non-typhoidal Salmonellosis obtained with different types of oral vaccines in different laboratories varies extensively (*38*). Our data

indicate that the variable efficacy of *Salmonella* niche competitors in the microbiota of mice is a critical determinant of protective efficacy. Microbiota composition also varies extensively between humans and over time (*39*). The vaccine-enhanced competition approach should remove the lottery of natural niche-competitor abundance and allow robust protection or therapy in most treated individuals. A limitation we would like to highlight here is that, due to practical and ethical restrictions, we have worked over relatively short timescales. We have not addressed the longevity of vaccine-induced responses, nor potential within-host evolution of competitor strains that might be observed over months or years. In this context, we cannot exclude that very small, below-detection limit reservoirs of infection may re-emerge at very late time-points post-treatment, even in this very robust prophylaxis system.

Currently, we have focused on one strain of pathogenic *Salmonella* and one commensal *E. coli* strain. Given the extensive strain-level variation in antigenicity, pathogenicity and metabolism between gut bacterial pathogens (*40*), the identification of the most relevant vaccine compositions and niche competitors may not be a case of simple extrapolation. Beyond non-encapsulated *Enterobacteriaceae*, there are open challenges in determining what the most relevant bacterial surface antigens are for IgA targeting and/or for designing oral vaccine strategies that optimally induce such responses. For example, *C. difficile* produces an S-layer with highly polymorphic exposed epitopes which is challenging for vaccine design (*41*). *Klebsiella* species that have been implicated in exacerbating inflammatory bowel disease symptoms (*42*) are heavily encapsulated, likely requiring glycoconjugate vaccines for induction of relevant antibody responses (*43*). Further important future directions therefore include (i) improving the breadth and affinity/avidity of IgA responses induced and (ii) optimizing the design of niche competitors/competitor consortia.

In conclusion, we have identified a mechanism to prevent *Salmonella* colonization and achieve *E. coli* strain replacement in the gut. These results lay the foundation for targeted

242 treatments for bacterial infections in mammals, promising significant advancements in
243 medical science.

REFERENCES AND NOTES

1. C. J. L. Murray *et al.*, Global burden of bacterial antimicrobial resistance in 2019: a systematic analysis. *Lancet* **399**, 629-655 (2022).
2. B. Stecher, Establishing causality in Salmonella-microbiota-host interaction: The use of gnotobiotic mouse models and synthetic microbial communities. *Int J Med Microbiol* **311**, 151484 (2021).
3. M. K. Herzog *et al.*, Mouse models for bacterial enteropathogen infections: insights into the role of colonization resistance. *Gut Microbes* **15**, 2172667 (2023).
4. M. Sassone-Corsi, M. Raffatellu, No Vacancy: How Beneficial Microbes Cooperate with Immunity To Provide Colonization Resistance to Pathogens. *Journal of Immunology* **194**, 4081-4087 (2015).
5. K. Ilg *et al.*, O-Antigen-Negative Salmonella enterica Serovar Typhimurium Is Attenuated in Intestinal Colonization but Elicits Colitis in Streptomycin-Treated Mice. *Infect Immun* **77**, 2568-2575 (2009).
6. S. Khanna, E. Voth, Therapeutics for Clostridioides difficile infection: molecules and microbes. *Expert Rev Gastroenterol Hepatol* **17**, 903-911 (2023).
7. K. Moor *et al.*, High-avidity IgA protects the intestine by enchaining growing bacteria. *Nature* **544**, 498-502 (2017).
8. K. Moor *et al.*, Peracetic Acid Treatment Generates Potent Inactivated Oral Vaccines from a Broad Range of Culturable Bacterial Species. *Front Immunol* **7**, 34 (2016).
9. F. Bansept *et al.*, Enchained growth and cluster dislocation: A possible mechanism for microbiota homeostasis. *PLoS Comput Biol* **15**, e1006986 (2019).
10. M. Diard *et al.*, A rationally designed oral vaccine induces immunoglobulin A in the murine gut that directs the evolution of attenuated Salmonella variants. *Nature Microbiology* **6**, 830-841 (2021).
11. D. Gil, J. P. Bouche, Cole1-Type Vectors with Fully Repressible Replication. *Gene* **105**, 17-22 (1991).
12. B. Stecher *et al.*, Chronic Salmonella enterica serovar Typhimurium-induced colitis and cholangitis in streptomycin-pretreated Nramp1+/+ mice. *Infect Immun* **74**, 5047-5057 (2006).
13. D. M. Monack, D. M. Bouley, S. Falkow, Salmonella typhimurium persists within macrophages in the mesenteric lymph nodes of chronically infected Nramp1+/+ mice and can be reactivated by IFNgamma neutralization. *J Exp Med* **199**, 231-241 (2004).
14. M. Diard *et al.*, Stabilization of cooperative virulence by the expression of an avirulent phenotype. *Nature* **494**, 353-356 (2013).
15. M. Diard *et al.*, Antibiotic treatment selects for cooperative virulence of Salmonella typhimurium. *Curr Biol* **24**, 2000-2005 (2014).
16. J. M. Slauch, A. A. Lee, M. J. Mahan, J. J. Mekalanos, Molecular characterization of the oafA locus responsible for acetylation of Salmonella typhimurium O-antigen: oafA is a member of a family of integral membrane trans-acylases. *J Bacteriol* **178**, 5904-5909 (1996).
17. L. Maier *et al.*, Granulocytes Impose a Tight Bottleneck upon the Gut Luminal Pathogen Population during Salmonella Typhimurium Colitis. *PLOS Pathogens* **10**, e1004557 (2014).
18. C. Eberl *et al.*, E. coli enhance colonization resistance against Salmonella Typhimurium by competing for galactitol, a context-dependent limiting carbon source. *Cell Host Microbe* **29**, 1680-1692.e1687 (2021).
19. E. Gül *et al.*, Differences in carbon metabolic capacity fuel co-existence and plasmid transfer between Salmonella strains in the mouse gut. *Cell Host Microbe* **31**, 1140-1153.e1143 (2023).
20. B. Stecher *et al.*, Like will to like: abundances of closely related species can predict susceptibility to intestinal colonization by pathogenic and commensal bacteria. *PLoS Pathog* **6**, e1000711 (2010).

21. S. Y. Wotzka *et al.*, Escherichia coli limits Salmonella Typhimurium infections after diet shifts and fat-mediated microbiota perturbation in mice. *Nature Microbiology* **4**, 2164-2174 (2019).
22. P. Kaiser, E. Slack, A. J. Grant, W.-D. Hardt, R. R. Regoes, Lymph Node Colonization Dynamics after Oral Salmonella Typhimurium Infection in Mice. *PLOS Pathogens* **9**, e1003532 (2013).
23. V. Liévin-Le Moal, A. L. Servin, Anti-infective activities of lactobacillus strains in the human intestinal microbiota: from probiotics to gastrointestinal anti-infectious biotherapeutic agents. *Clin Microbiol Rev* **27**, 167-199 (2014).
24. R. Ravindran, J. Foley, T. Stoklasek, L. H. Glimcher, S. J. McSorley, Expression of T-bet by CD4 T cells is essential for resistance to Salmonella infection. *J Immunol* **175**, 4603-4610 (2005).
25. S. K. Hoiseth, B. A. Stocker, Aromatic-dependent Salmonella typhimurium are non-virulent and effective as live vaccines. *Nature* **291**, 238-239 (1981).
26. P. Kaiser *et al.*, Cecum lymph node dendritic cells harbor slow-growing bacteria phenotypically tolerant to antibiotic treatment. *PLoS Biol* **12**, e1001793 (2014).
27. K. Endt *et al.*, The Microbiota Mediates Pathogen Clearance from the Gut Lumen after Non-Typhoidal Salmonella Diarrhea. *PLOS Pathogens* **6**, e1001097 (2010).
28. L. Maier *et al.*, Microbiota-derived hydrogen fuels Salmonella typhimurium invasion of the gut ecosystem. *Cell Host Microbe* **14**, 641-651 (2013).
29. M. G. Netea *et al.*, Trained immunity: A program of innate immune memory in health and disease. *Science* **352**, aaf1098 (2016).
30. J. M. Pickard, G. Núñez, Pathogen Colonization Resistance in the Gut and Its Manipulation for Improved Health. *Am J Pathol* **189**, 1300-1310 (2019).
31. M. T. Sorbara, E. G. Pamer, Interbacterial mechanisms of colonization resistance and the strategies pathogens use to overcome them. *Mucosal Immunol* **12**, 1-9 (2019).
32. F. Spragge *et al.*, Microbiome diversity protects against pathogens by nutrient blocking. *Science* **382**, eadj3502 (2023).
33. S. Brugiroux *et al.*, Genome-guided design of a defined mouse microbiota that confers colonization resistance against Salmonella enterica serovar Typhimurium. *Nat Microbiol* **2**, 16215 (2016).
34. N. Kumar, T. C. A. Hitch, D. Haller, I. Lagkouvardos, T. Clavel, MiMiC: a bioinformatic approach for generation of synthetic communities from metagenomes. *Microb Biotechnol* **14**, 1757-1770 (2021).
35. V. Melkebeek, B. M. Goddeeris, E. Cox, ETEC vaccination in pigs. *Veterinary Immunology and Immunopathology* **152**, 37-42 (2013).
36. S. D. Isidean, M. S. Riddle, S. J. Savarino, C. K. Porter, A systematic review of ETEC epidemiology focusing on colonization factor and toxin expression. *Vaccine* **29**, 6167-6178 (2011).
37. J. N. V. Martinson *et al.*, Rethinking gut microbiome residency and the Enterobacteriaceae in healthy human adults. *Isme j* **13**, 2306-2318 (2019).
38. F. Fransen *et al.*, BALB/c and C57BL/6 Mice Differ in Polyreactive IgA Abundance, which Impacts the Generation of Antigen-Specific IgA and Microbiota Diversity. *Immunity* **43**, 527-540 (2015).
39. G. McCallum, C. Tropini, The gut microbiota and its biogeography. *Nat Rev Microbiol* **22**, 105-118 (2024).
40. D. Yu, G. Banting, N. F. Neumann, A review of the taxonomy, genetics, and biology of the genus Escherichia and the type species Escherichia coli. *Can J Microbiol* **67**, 553-571 (2021).
41. K. E. Dingle *et al.*, Recombinational switching of the Clostridium difficile S-layer and a novel glycosylation gene cluster revealed by large-scale whole-genome sequencing. *J Infect Dis* **207**, 675-686 (2013).
42. S. Federici *et al.*, Targeted suppression of human IBD-associated gut microbiota commensals by phage consortia for treatment of intestinal inflammation. *Cell* **185**, 2879-2898.e2824 (2022).
43. L. Assoni, R. Girardello, T. R. Converso, M. Darrieux, Current Stage in the Development of Klebsiella pneumoniae Vaccines. *Infect Dis Ther* **10**, 2157-2175 (2021).

44. V. Lentsch. (ETH Zurich, 2025).
45. A. J. Grant *et al.*, Modelling within-host spatiotemporal dynamics of invasive bacterial disease. *PLoS Biol* **6**, e74 (2008).
46. B. Stecher *et al.*, Gut inflammation can boost horizontal gene transfer between pathogenic and commensal Enterobacteriaceae. *Proc Natl Acad Sci U S A* **109**, 1269-1274 (2012).
47. A. Rasko David *et al.*, The Pangenome Structure of Escherichia coli: Comparative Genomic Analysis of E. coli Commensal and Pathogenic Isolates. *Journal of Bacteriology* **190**, 6881-6893 (2008).
48. S. Hapfelmeier *et al.*, The Salmonella pathogenicity island (SPI)-2 and SPI-1 type III secretion systems allow Salmonella serovar typhimurium to trigger colitis via MyD88-dependent and MyD88-independent mechanisms. *J Immunol* **174**, 1675-1685 (2005).
49. L. M. Guzman, D. Belin, M. J. Carson, J. Beckwith, Tight regulation, modulation, and high-level expression by vectors containing the arabinose PBAD promoter. *J Bacteriol* **177**, 4121-4130 (1995).
50. P. P. Cherepanov, W. Wackernagel, Gene disruption in Escherichia coli: TcR and KmR cassettes with the option of Flp-catalyzed excision of the antibiotic-resistance determinant. *Gene* **158**, 9-14 (1995).
51. Y. Zhang *et al.*, Multicopy Chromosomal Integration Using CRISPR-Associated Transposases. *ACS Synth Biol* **9**, 1998-2008 (2020).
52. G. J. McKenzie, N. L. Craig, Fast, easy and efficient: site-specific insertion of transgenes into Enterobacterial chromosomes using Tn7 without need for selection of the insertion event. *BMC microbiology* **6**, 39 (2006).
53. K. A. Datsenko, B. L. Wanner, One-step inactivation of chromosomal genes in Escherichia coli K-12 using PCR products. *Proc Natl Acad Sci U S A* **97**, 6640-6645 (2000).
54. N. L. Sternberg, R. Maurer, Bacteriophage-mediated generalized transduction in Escherichia coli and Salmonella typhimurium. *Methods Enzymol* **204**, 18-43 (1991).
55. M. Sobota *et al.*, The expression of virulence genes increases membrane permeability and sensitivity to envelope stress in Salmonella Typhimurium. *PLOS Biology* **20**, e3001608 (2022).
56. E. Bakkeren *et al.*, Impact of horizontal gene transfer on emergence and stability of cooperative virulence in Salmonella Typhimurium. *Nat Commun* **13**, 1939 (2022).
57. K. Moor *et al.*, Analysis of bacterial-surface-specific antibodies in body fluids using bacterial flow cytometry. *Nat Protoc* **11**, 1531-1553 (2016).

Acknowledgements: We thank Benoit Pugin for providing the *Lactobacillus casei* strains used in this work. We thank Kevin Foster, Daniel Hoces and Markus Arnoldini, and members of the Slack lab for helpful discussions and comments, Yassine Cherrak and Ersin Gül for technical advice, Ronja Rappold, Alice de Wouters d'Oplinter, Kateryna Vershynina, Suwannee Ganguillet and Leonardo Rocha for their support in experiments, and the staff at the RCHCI, EPIC and Biozentrum animal facilities for their excellent support.

Funding: Funding for this work was provided by the Gebert Rüf Microbials (GR073_17). VL, AW, CL and ES are supported by the Gebert Rüf Microbials (GR073_17). ES acknowledges the support of the Swiss National Science Foundation (40B2-0_180953,

310030_185128), and European Research Council Consolidator Grant (865730). This work was supported as a part of NCCR Microbiomes, a National Centre of Competence in Research, funded by the Swiss National Science Foundation (grant number 180575). Funding was provided by the Botnar Research Centre for Child Health as part of the Multi-Investigator Project: Microbiota Engineering for Child Health. ES is supported by the LOOP Zurich mTORUS project. MD is supported by a SNF professorship (PP00PP_176954) and Gebert Rüf Microbials (PhagoVax GRS-093/20). WDH acknowledges funding by grants from the Swiss National Science Foundation (310030_192567, NCCR Microbiomes). CL is supported by Agence Nationale de la Recherche (ANR-21-CE45-0015, 376 ANR-20-CE30-0001) and MITI CNRS AAP adaptation du vivant à son environnement.

Author contributions: Conceptualization, V.L., M.D., E.S.; Investigation, V.L., A.W., A.R., S.A., C.M., S.A.F., N.R., N.W., L.L., E.C.B., M.D.; Methodology, V.L., A.W., C.L.; Software, A.W., C.L.; Validation, V.L., A.W., C.M.; Data Curation, V.L., A.W., C.M.; Formal Analysis, V.L., A.W., C.L.; Project administration, V.L. E.S.; Funding acquisition, M.D. E.S.; Resources, W-D.H., C.L. E.S.; Supervision, V.L., W-D.H., C.L., M.D., E.S.; Visualization, V.L., A.W.; Writing – original draft, V.L., E.S.; Writing – review and editing, V.L., A.W., A.R., C.M., S.A., N.R., S.A.F., N.W., L.L., W-D.H., C.L., M.D., E.S.;

Competing interests: Patents: Verena Lentsch, Médéric Diard and Emma Slack are inventors on patent/patent application EP22186078.6 submitted by the University of Basel and ETH Zurich that covers combining a genetically engineered probiotic niche competitor and vaccination related to this work. Verena Lentsch, Médéric Diard and Emma Slack are inventors on patent/patent application EP24208390 submitted jointly by the University of

Basel and ETH Zurich that covers combining probiotic niche competitors, vaccination and bacteriophage treatment, related to this work. No commercial development is currently associated with these patents and no financial conflict of interest exists.

Data and Materials availability: Original code and raw data have been deposited at ETH Zurich Research Collection https://doi.org/10.3929/ethz-b-000717590(*44*). Newly generated bacterial strains and all other materials are available from Emma Slack (emma.slack@hest.ethz.ch) and Médéric Diard (mederic.diard@biozentrum.unibas.ch).

List of Supplementary Materials

Materials and Methods

Supplementary Modelling Text

Figures S1 to S12

Tables S1 to S8

References (*46-56*)

Figure titles and legends

Figure 1. Vaccine-enhanced competition based on an inactivated whole-cell oral vaccination and *S*.Tm^{Comp} can eliminate *S*.Tm^{WT} from the gut and prevent *S*.Tm^{WT} transmission. (**A**) Experimental procedure. PBS (blue) or PA-*S*.Tm-vaccinated (pink) 129S6/SvEv mice were pretreated with streptomycin and infected with $1{\cdot}10^6$ *S*.Tm^{WT}. Indicated groups were pre-colonized with $5{\cdot}10^3$ *S*.Tm^{Comp} at day -3 (filled symbols). (**B**) *S*.Tm^{WT}-specific intestinal IgA titres at endpoint. *S*.Tm CFUs in cecum content (**C**), feces (**D**) MLN (**E**) and spleen (**F**). *S*.Tm^{WT}-free mice in (**D**) refers to Vacc.+*S*.Tm^{Comp} group. (**G-I**) Intestinal inflammation determined by fecal lipocalin-2 (**G**) and cecum histopathological scoring (**H**). (**I**) Representative images of H&E-stained cecum. Arrowheads indicate goblet cells. Scale: 100 µm. (**J-K**) Streptomycin-pretreated naïve 129S6/SvEv mice received a FMT with feces collected on day 9 from A-K. *S*.Tm^{WT} and *S*.Tm^{Comp} CFUs in feces (**J**) and cecum content (**K**). The pink open triangle depicts a donor from the Vacc.+*S*.Tm^{Comp} group in which *S*.Tm^{WT} transmission occurred.

Pooled data from two independent experiments with switched antibiotic resistances (n=5-8 mice/group (A-I) or n=8 mice/group (J-K)).

Solid lines: median. error bars: interquartile range. Dotted lines: detection limit. Shaded area: detection limit range. Open triangles: (n=1) euthanized prematurely due severe disease. One-way ANOVA (H) performed on log-normalized data (B-C, E-F) or area under the curve (AUC) (D, G). Unpaired two-tailed t-test performed on log-normalized data (B-C, E-F). DF, dilution factor; Lu., lumen; MFI, median fluorescence intensity; S.E., submucosal edema.

Figure 2. Metabolic niche overlap of *S*.Tm^{WT} and *S*.Tm^{Comp} favours vaccine-enhanced competition. (**A**) Experimental procedure. PBS or PA-*S*.Tm-vaccinated 129S6/SvEv mice were pre-colonized with $5{\cdot}10^3$ *S*.Tm^{Comp} or *S*.Tm$^{Comp\Delta gatABC}$ 3 days before infection and infected with a 1:1 ratio of $1{\cdot}10^6$ *S*.Tm^{WT} and *S*.Tm$^{\Delta gatABC}$. (**B**) *S*.Tm CFUs in feces (n=5 mice/group). Solid lines: median, error bars: interquartile range. Dotted lines/shading: detection limit and range. Two-way ANOVA on log-normalized data between *S*.Tm^{WT} and *S*.Tm$^{\Delta gatABC}$ and one-way ANOVA on AUC comparing *S*.Tm^{WT} between treatment groups was performed.

Figure 3. Vaccine-enhanced competition with an imperfect niche competitor limits *S*.Tm^{WT} colonization and prevents inflammation. (**A**) Experimental procedure. PBS (blue) or EvoVax vaccinated (pink) 129S6/SvEv mice were pretreated with ampicillin and infected

with $1 \cdot 10^6$ *S*.Tm^{WT}. Two groups were pre-colonized with $5 \cdot 10^3$ *E. coli* 8178 3 days before infection. (**B-E**) CFUs in feces (**B**), cecum content (**C**), liver (**D**) and spleen (**E**). Intestinal inflammation determined by fecal lipocalin-2 (**F**) and histopathological scoring of cecum (**G**). (**H**) Representative images of H&E-stained cecum. Arrowheads show goblet cells. Scale bars: 100 µm.

Pooled data from two independent experiments (n=6-8 mice/group). Solid lines: median, error bars: interquartile range. Dotted lines and shading: detection limit and range (when detection limit depends on sample weight). Open triangles: mice (n=3) euthanized due to excessive pathology. One-way ANOVA (E) on log-normalized data (C) or area under the curve (AUC) (B-D). Unpaired two-tailed t-test on log-normalized data for comparing 2 groups (C).

Figure 4. Vaccine-enhanced competition can be used to therapeutically replace a gut *E. coli* strain. (**A**) Experimental procedure. C57BL/6 low-complexity microbiota mice were colonized with the commensal *E. coli* HS strain. 3 days later, vaccination with either vehicle alone or PA-*E. coli* HS was started and a cocktail of competitor *E. coli* was introduced orally on day 10 and 17. (**B**) Intestinal IgA titres specific for *E. coli* HS and the competitor strains at endpoint. (**C**) Fecal and (**D**) cecal CFUs. Pooled data from two independent experiments (n=6-10 mice/group). Solid lines: median, error bars: interquartile range. Dotted lines and shading: detection limit and range. One-way ANOVA on log-normalized data (B, D) or area under the curve (AUC) (C).

Figure 5. Therapeutic clearance of *E. coli* is antibody dependent. (**A**) Experimental procedure. C57BL/6 "low-complexity microbiota" mice were colonized with *E. coli* HS. 3 days later, vaccination with either vehicle alone or PA-*E. coli* HS was started, and a cocktail of competitor *E. coli* was introduced orally on day 10 and 17. Mice were treated with anti-CD4 and anti-CD20 or isotype controls one day before vaccination. (**B**) $CD4^+$ T cells and B cells in blood at endpoint. (**C**) *E. coli* HS-specific intestinal IgA titres at endpoint. (**D**) Fecal and (**E**) cecal CFUs. Pooled data from two independent experiments (n=4-5 mice/group). Solid lines: median. error bars: interquartile range. Dotted lines and shading: detection limit and range. One-way ANOVA (B) on log-normalized data (C, E) or area under the curve (AUC) (D).

Figure 1. Vaccine-enhanced competition based on an inactivated whole-cell oral vaccination and *S*.Tm^{Comp} can eliminate *S*.Tm^{WT} from the gut and prevent *S*.Tm^{WT} transmission.

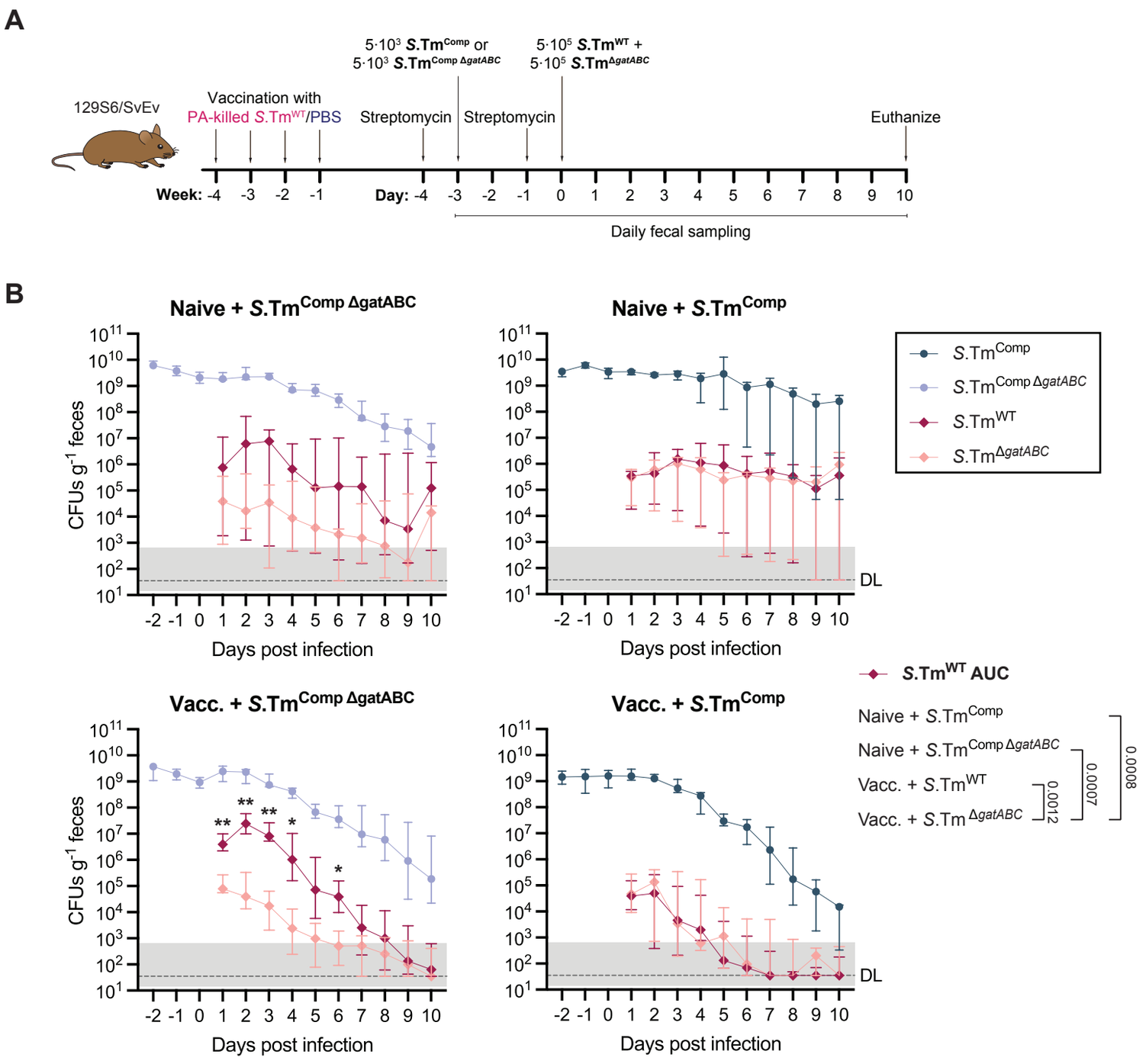

Figure 2. Metabolic niche overlap of *S*.Tm^{WT} and *S*.Tm^{Comp} favours vaccine-enhanced competition.

Figure 3. Vaccine-enhanced competition with an imperfect niche competitor suppresses *S*.Tm^{WT} colonization and inflammation.

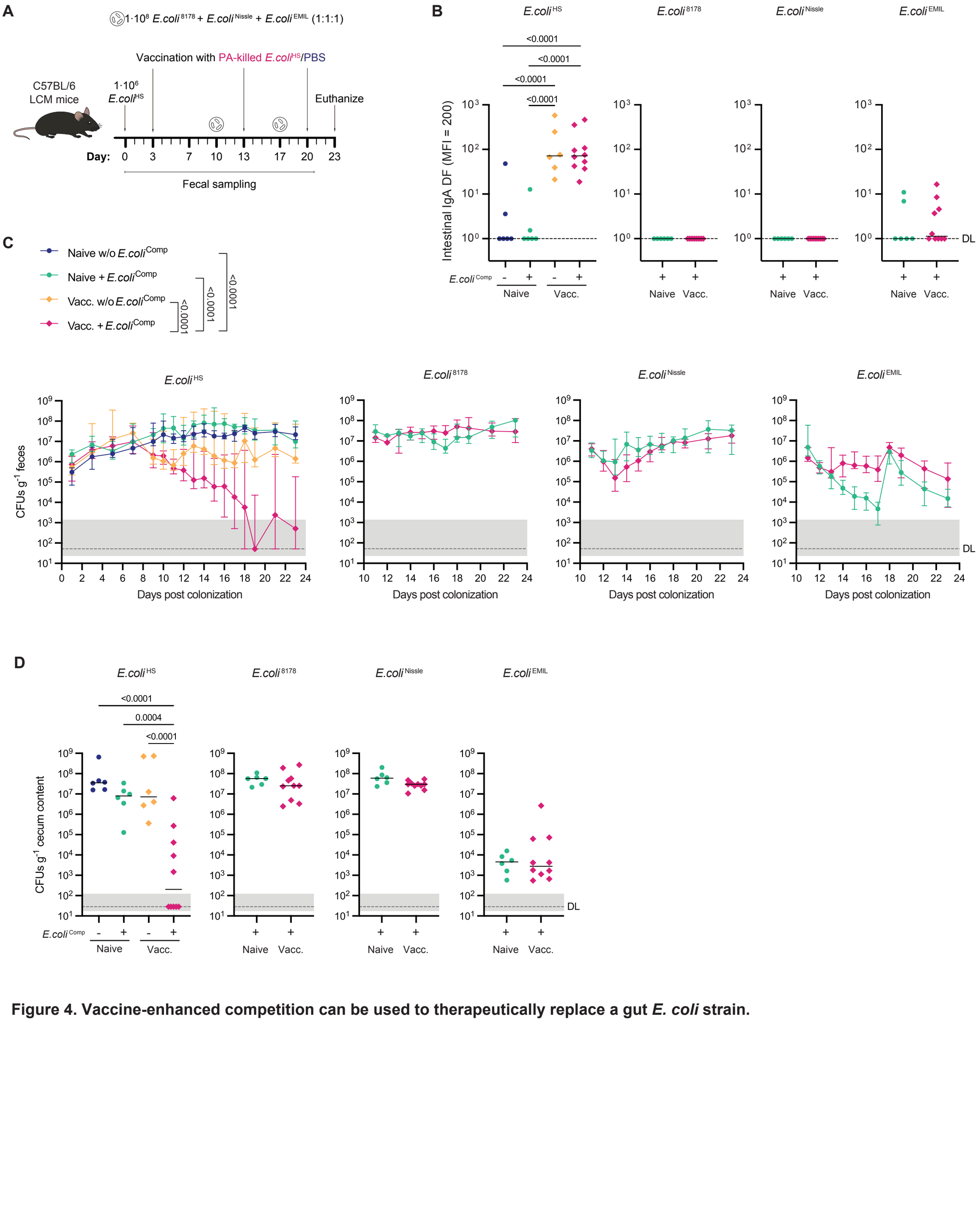

Figure 4. Vaccine-enhanced competition can be used to therapeutically replace a gut *E. coli* strain.

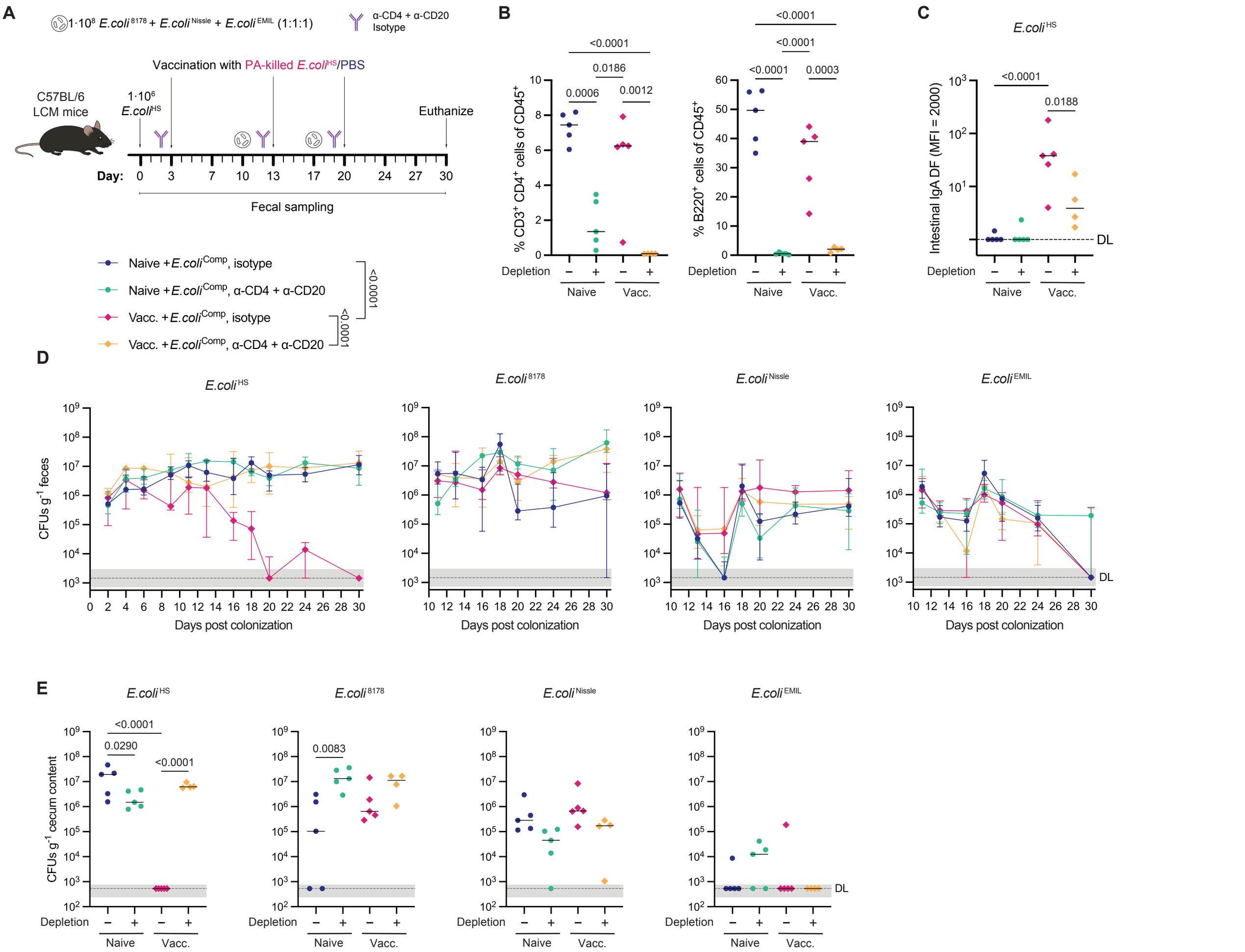

Figure 5. Therapeutic clearance of *E. coli* is antibody dependent.

Science
AAAS

450

Supplementary Materials for

Title: Vaccine-enhanced competition permits rational bacterial strain replacement in the gut

Authors: Verena Lentsch, Aurore Woller, Andrea Rocker, Selma Aslani, Claudia Moresi, Niina Ruoho, Louise Larsson, Stefan A. Fattinger, Nicolas Wenner, Elisa Cappio Barazzone, Wolf-Dietrich Hardt, Claude Loverdo, Médéric Diard, Emma Slack

Corresponding author: emma.slack@hest.ethz.ch

The PDF file includes:

Materials and Methods

Figs. S1 to S12

Tables S1 to S8

Supplementary References

Materials and Methods

Strains and plasmids

All strains and plasmids used in this study are listed in table S1.

Table S1. Strains and plasmids used in this study.

Strains	Strain number	Relevant genotype	Resistance	Reference
S.Tm^{WT}	SB300	SL1344, Wild-type	Sm	(*25*)
S.Tm TAG13 *aphT*		WITS13-*aphT*	Sm, Kan	(*45*)
S.Tm TAG13 *cat*		WITS13-*cat*	Sm, Cm	(*45*)
S.Tm^{Comp}	A58	Δ*oafA* Δ*hilD ssaV*::*aphT*	Sm, Kan	This work
S.Tm^{Comp}	B62	Δ*ssaV* Δ*oafA* Δ*hilD marT*::*cat*	Sm, Cm	This work
S.Tm$^{\Delta gatABC}$		Δ*gatABC* WITS2-*aphT*	Sm, Kan	(*19*)
S.Tm$^{Comp\ \Delta gatABC}$	F78	Δ*ssaV* Δ*oafA* Δ*hilD* Δ*gatABC* Tn7::*aac3-VI*	Apra	This work
E. coli 8178 p2^{cured}		p2 cured		(*46*)
E. coli Nissle		Nissle 1917 wild-type	Sm	(*46*)
E. coli HS, WT		Wild-type		(*47*)
E. coli HS	MDBZ1822	Tn7::*aphT*	Kan	This work
E. coli EMIL, WT	MDBZ1611	Wild-type, ST602 commensal strain		This work
E. coli EMIL	MDBZ1775	Tn7::*cat*	Cm	This work
L. casei WS01.02			Sm, Pen	FAM
L. casei WS20.11			Sm, Pen, Tet	FAM
S.Tm^{aroA}	D12	Δ*aroA* WITS13-*cat*	Sm, Cm	This work
Plasmids	**Used in**	**Description**	**Resistance**	**Reference**
pAM34	*S*.Tm^{WT} and *S*.Tm^{Comp}	ColE type vector requiring IPTG for replication	Amp	(*11*)
pM975	*S*.Tm^{WT} and *Ec*^{8178}	used to confer ampicillin resistance	Amp	(*48*)
pBAD24	*S*.Tm^{WT} and *Ec*^{8178}	used to confer ampicillin resistance	Amp	(*49*)
pCP20		FLP recombinase	Amp, Cm	(*50*)
pCutamp	Template for *aac3-VI* cassette	The plasmid harboring SpCas9, SacB and sgRNA targeting Amp promote	Apra	(*51*)
pGRG36	Tn*7* tagging	Mini-Tn*7* delivery plasmid, temperature-sensitive origin from pSC101	Amp	(*52*)
pGRG36-*aac3-VI*	Tn*7*:: *aac3-VI* tagging	pGRG36 derivative, mini-Tn*7* ::*aphT* delivery plasmid	Amp, Apra	This work
pGRG36-*aphT*	Tn*7*::*aphT* tagging	pGRG36 derivative, mini-Tn*7* ::*aphT* delivery plasmid	Amp,Km	This work
pGRG36-*cat*	Tn*7*::*cat* tagging	pGRG36 derivative, mini-Tn*7* ::*cat* delivery plasmid	Amp,Cm	This work
pKD3	Template for *cat* cassette	*frt-cat-frt* template plasmid	Cm	(*53*)

pKD4	Template for *aphT* cassette	*frt-aphT-frt* template plasmid	Km	(*53*)

All *E. coli* and *S*.Tm were cultivated in lysogeny broth (LB) containing appropriate antibiotics (100 µg/ml streptomycin (Sm, AppliChem); 15 µg/ml chloramphenicol (Cam, AppliChem); 50 µg/ml kanamycin (Kan, AppliChem); 50 µg/ml ampicillin (Amp, AppliChem), 50 µg/ml apramycin (Apra, Sigma-Aldrich). *L. casei* (isolates from the Swiss Federal Dairy Research Station (FAM), Liebefeld) was grown in De Man–Rogosa–Sharpe (MRS) Broth + 0.2% Tween 80 containing appropriate antibiotics. Dilutions were prepared in Phosphate Buffered Saline (PBS, Difco).

Gene-deletion mutants in *Salmonella* were created by generalized transduction with bacteriophage P22 HT105/1 *int-201* in an *S*.Tm SL1344 background as described in(*54*), using pre-existing mutants marked with antibiotic resistances. When needed, antibiotic resistance cassettes were removed using the temperature sensitive FLP recombinase encoded on pCP20 (*50*). Deletions originated from in-frame deletions made in *S*.Tm 14028S, kind gifts from Prof. Michael McClelland (University of California, Irvine). Primers used for verifications of gene deletions or genetic background are listed in table S2.

In order to chromosomally tag *E. coli* and *Salmonella* strains with Tn*7* transposons carrying distinct resistance genes, three plasmids derived from the mini-Tn*7* delivery plasmid pGRG36 (*51*) were constructed. The *aphT* (Km^R), *aac3-VI* ($Apra^R$) or *cat* (Cm^R) resistance genes were PCR-amplified (Phusion DNA polymerase, ThermoFisher) from template plasmids pKD4, pCutamp or pKD3 with primer pairs aphT-Tn7_Fw/Rv, ApmR-Tn7_Fw/Rv or cat-Tn7_Fw/Rv, respectively. The resulting blunt-end PCR fragments were inserted into the mini-Tn*7* of plasmid pGRG36, as follows: pGRG36 was linearized with SmaI (NEB) and the resistance genes were ligated using T4 DNA Ligase (NEB). The ligation reactions were transformed into electro-competent *E. coli* DH5α cells and colonies carrying the plasmids pGRG36-*aphT*, pGRG36- *aac3-VI* or pGRG36-*cat* were selected at 30° C on LB agar plates supplemented with Km, Apra or Cm, respectively. The resistance gene sequences and orientation in the resulting plasmids were checked by Sanger sequencing, using primers Tn7L_Fw and Tn7L_Rv. The Tn*7* transposons carrying the antibiotic resistance were inserted downstream of chromosomal gene *glmS*, using the methodology described by McKenzie and Craig (*52*). Finally, the temperature sensitive pGRG36 plasmids were eliminated by a passage at 42° C and site-specific insertions of Tn*7* were confirmed by PCR and Sanger sequencing using primer pairs glms_check_fw/rv for *E. coli* or glmS_Sal_check_fw/rv for *Salmonella*.

E. coli EMIL was isolated from the microbiota of a contaminated 129S6/SvEvTac WT mouse cage. Genome comparison identified it to belong to the ST602 sequence type.

Table S2. Primers used in this study.

Primer name	Sequence (5' - 3')	Purpose	Reference
hilD_fw	TCTCGATAGCAGCAGATTAC	Deletion verification hilD	(*55*)
hilD_rv	CAGTATAAGCTGTCTTCCG		(*55*)
oafA_fw	CCGCCATAGTTACGTTTTG	Deletion verification oafA	(*10*)
oafA_rv	AAGCTATACACATAAAATAATTTGC		(*10*)
ssaV_fw	GCAGCGTTCCAGGGTATTCC	Deletion verification ssaV	(*56*)
ssaV_rv	CAGCAAGTTCTTCTCCAGGC		(*56*)
aroA_fw	CATGATCGATTTTGAGCGT	Deletion verification aroA	This study
aroA_rv	ATAGTGCGAATACGGACTCG		This study
marT_fw	AGCCCTACACCCAGACACAG	Deletion verification marT	This study
marT_rv	GCCACAGCATCAGACTATAC		This study
gatABC_fw	CTGAACAACGTCACATTGCC	Deletion verification gatABC	(*19*)
gatABC_rv	CTCAGCGTGAATAACCACTG		(*19*)
ApmR-Tn7_Fw	GGGGACGTCCCGCGGCTGACGCCGTTGGATAC	Construction of pGRG36-*aac3-VI*	This study
ApmR-Tn7_Rv	GATGAGCTCAGCCAATCGAC		This study
aphT-Tn7_Fw	GGGGACGTCCCGCGGGCGCAAGGGCTGCTAAAG	Construction of pGRG36-*aphT*	This study
aphT-Tn7_Rv	GTCCCGCTCAGAAGAACTCG		This study
cat-Tn7_Fw	GGGGACGTCCCGCGGCGCGCCTACCTGTGACGGA	Construction of pGRG36-*cat*	This study
cat-Tn7_Rv	TTACGCCCCGCCCTGCCACT		This study
Tn7L_Fw	GGGAACTGGGTGTAGCGTCG	Sequencing in pGRG36	This study
Tn7R_Rv	GGCGGACAATAAAGTCTTAAAC		This study
glms_check_fw	GCATGTGGAAGAGGTGATTG	PCR-check of Tn*7* insertion in the *glmS-pstS* locus of *E. coli*	This study
glms_check_rv	AATGTCTCCTGGGAGGATTC		This study
glmS_Sal_check_fw	CGTTCCGCTGCAACTGCTGG	PCR-check of Tn*7* insertion in the *glmS-STM3860* locus of *Salmonella*	This study
glmS_Sal_check_rv	ATCCACCTGAATAACCTGGG		This study

Plasmids were transferred by electro-transformation into competent cells (*39, 44*).

Mice

All animal experiments were performed in accordance with Swiss Federal regulations approved by the Commission for Animal Experimentation of the Kanton Zurich or Basel-Stadt (licenses 193/2016, 158/2019, 120/2019, and 109/2022; Kantonales Veterinäramt Zürich, Switzerland and licences #30480 and #33580; Basel-Stadt Kantonales Veterinäramt, Switzerland). Specific opportunistic pathogen-free (SPF, containing a complete microbiota free of an extended list of opportunistic pathogens) 129S6/SvEvTac WT mice were used in all experiments except for fig. S2 A-F, where C57BL/6J WT mice and Fig. 4 and 5 where low-complexity microbiota (LCM) C57BL/6J WT mice were used (*30*). Mice were bred and housed in individually ventilated cages with a 12 h light/dark cycle in the ETH Phenomics Center (EPIC, RCHCI), ETH Zürich or at Biozentrum Basel, University of Basel. All mice used in the experiments were *E. coli* free, as determined by plating of feces. All mice were maintained on standard chow (Kliba Nafag, 3537; autoclaved; per weight: 4.5% fat, 18.5% protein, ~50% carbohydrates, 4.5% fibre). As indicated, mice were shifted to a high fat diet without fibre (HFD; BioServ, S3282; 60% kcal fat; irradiated; per weight: 36% fat, 20.5% protein, 35.7% carbohydrates, 0% fibre). All mice included

in experiments were 4 weeks or older and objectively healthy as determined by routine health checks. Wherever possible an equal number of males and females was used in each group. Mice were allocated cage-wise to groups with a minimum of two cages per group. As strong phenotypes were expected, we adhered to standard practice of analysing at least five mice per group. Researchers were not blinded to group allocation to decrease the risk of contamination and because the majority of readouts were quantitative and not subjective (CFU determination, ELISA). The one exception to this was histopathology scoring, for which a blinded researcher (S.A.F.) not otherwise involved in the experiment carried out all scoring. All animals were euthanized by exposure to a slowly rising carbon dioxide concentration, followed by exsanguination to confirm death.

Vaccinations

Mice were orally vaccinated with peracetic acid (PA) killed vaccines unless otherwise specified.

Peracetic acid killed vaccines were produced as previously described (*8*). Briefly, bacteria were grown overnight to late stationary phase, harvested by centrifugation and re-suspended to a density of 10^9-10^{10} per ml in sterile PBS. Peracetic acid (Sigma-Aldrich) was added to a final concentration of 0.4% v/v. The suspension was mixed thoroughly and incubated for 60 min at room temperature. Bacteria were washed three times in 50-100 ml sterile PBS. The final pellet was resuspended to yield a density of 10^{11}-10^{12} particles per ml in sterile PBS. The exact number was determined by flow cytometry with counting beads (Fluoresbrite® Multifluorescent Microspheres). Vaccines were stored at 4 °C for up to six weeks. Each batch of vaccine was tested for sterility before use. Vaccine lots were released for use only when a negative enrichment culture had been confirmed. Mice were vaccinated with 10^{10}-10^{11} PA-killed bacteria by oral gavage or voluntary feeding, once weekly for 4 weeks. Where multiple strains were used for vaccination, 10^{10}-10^{11} of each strain were mixed and given as a single dose.

For the one experiment series with live-attenuated *S*.Tm^{aroA} vaccination, the vaccine strain was grown overnight in LB containing chloramphenicol. The cells were washed in PBS and resuspended at a density of 10^{10} bacteria per ml. Mice were orally vaccinated with 10^9 *S*.Tm^{aroA} in 100 µl three times in bi-weekly intervals without antibiotic pretreatment.

Vaccinations were started in mice at an age of 4-6 weeks.

Bacterial competitor colonizations and *Salmonella* challenge infections

The competitor strain was grown overnight in LB containing the appropriate antibiotics. In the morning, the bacteria were washed with sterile PBS and diluted. The competitor was introduced by oral gavage into the respective groups as stated in the respective figures.

Non-typhoidal *Salmonella* infections were carried out as previously described (*12*). In brief, mice were orally pretreated 24 h before infection with 25 mg (roughly 1 mg/g body weight) streptomycin or 20 mg (roughly 0.8 mg/g body weight) ampicillin. Strains were cultivated overnight separately in LB containing the appropriate antibiotics. Subcultures were prepared before infections by diluting overnight cultures 1:20 in fresh LB without antibiotics and incubation for 3 h at 37 °C to produce an inoculum in late-log phase growth. The cells were washed in PBS, diluted, and 100 µl of bacteria were used to infect mice by orogastric gavage, as indicated in the respective figure legends/text. A detailed layout of the vaccination and infection schedule is shown in the figures.

Salmonella infections in high-fat diet treated mice were carried out similarly, but instead of antibiotic treatment, all mice were switched to a high-fat diet (described above) 24 h prior to challenge.

For the murine typhoid model, no pretreatment is given and *Salmonella* infection is carried out with $5x10^7$ CFU per mouse given by orogastric gavage.

Feces were sampled daily, homogenized in 500 µl PBS by bead beating (3 mm steel ball, 25 Hz for 2.5 min in a TissueLyser (Retsch)), and large particles were sedimented by centrifugation at 500x *g* for 1 minute. Bacteria were enumerated by selective plating on MacConkey agar, MRS agar or LB Agar supplemented with the appropriate antibiotics. Fecal samples for lipocalin-2 measurements were kept homogenized in PBS at -20 °C. At endpoint, blood was collected from the heart into 1.1 ml serum gel tubes (Sarstedt). Intestinal lavages were harvested by flushing the small intestinal content with 2 ml of PBS using a cannula. The middle part of the cecum was placed into OCT Compound (Tissue-Tek), snap-frozen and stored at -80 °C until analysis. Spleen, liver, mesenteric lymph nodes were collected and homogenized in 1 ml PBS at 30 Hz for 3 min. Cecum content was collected and homogenized in 500 µl PBS at 25 Hz for 2.5 min. After centrifugation at 500x *g* for 1 minute, bacteria were plated on selective MacConkey agar.

Bacterial competitor colonizations and *E. coli* HS clearance

E. coli HS was grown overnight in LB containing the appropriate antibiotics. In the morning, the bacteria were washed with sterile PBS and diluted. The *E. coli* HS was introduced by oral gavage into all groups of low-complexity microbiota C57BL/6 mice on day 0.

From day 3, mice received a once weekly vaccination of 10^{10} particles of peracetic acid-killed *E. coli* HS. On day 10 and day 17, mice received a cocktail of three competitor *E. coli* strains (*E. coli*^{8178}, *E. coli*$^{\text{Nissle}}$, *E.* coli$^{\text{EMIL}}$). A detailed layout of the vaccination and infection schedule is shown in the figures.

Feces were sampled daily, homogenized in 500 µl PBS by bead beating (3 mm steel ball, 25 Hz for 2.5 min in a TissueLyser (Retsch)), and large particles were sedimented by centrifugation at 500x *g* for 1 minute. Bacteria were enumerated by selective plating on MacConkey agar, MRS agar or LB Agar supplemented with the appropriate antibiotics. At endpoint, blood was collected from the heart into 1.1 ml serum gel tubes (Sarstedt). Intestinal lavages were harvested by flushing the small intestinal content with 2 ml of PBS using a cannula.

B and T cell depletion

For $CD4^+$ T cell and B cell depletion during *S*.Tm and *E. coli* vaccinations, mice were injected i.p. with 100 µg anti-CD4 (GK 1.5, Bioxcell, BE0003-1) and anti-CD20 (MB20-11, Bioxcell, BE0356) or 100 µg rat IgG2b isotype control (LTF-2, Bioxcell, BE0090) and mouse IgG2c isotype control (DV5-1, Bioxcell BE0366) one day prior to each vaccination.

For T cell depletion during *S*.Tm infection, mice were injected i.p. with 100 µg anti-CD4 (GK 1.5, Bioxcell, BE0003-1, AB_1107636) and anti-CD8α (2.43, Bioxcell, BE0061, AB_1125541) or 100 µg rat IgG2b isotype control (LTF-2, Bioxcell, BE0090, AB_1107780) one day prior to infection, and then every fourth day (for a total of three injections).

Confirmation of depletion

T and B cell depletions were confirmed in blood, spleen and mesenteric lymph nodes by flow cytometry. Spleens and MLNs were harvested and disintegrated using a 70 µm cell strainer (Falcon) to obtain a single cell suspension in FACS buffer (PBS, 2% FBS, 5 mM EDTA). Cells were washed twice and 1/5 was used for staining in 50 µl LIVE/DEAD™ Fixable Aqua Dye (ThermoFisher Scientific, L34957) diluted in FACS buffer. Cells were incubated at 4 °C for 20 min, washed and stained for cell surface markers. The following antibodies were used for surface staining: Alexa Fluor 488 anti-mouse CD3 (17A2, Biolegend, 1.25 µg/ml, 100210, AB_389301), Alexa Fluor 647 anti-mouse CD3 (17A2, Biolegend, 5 µg/ml, 100209, AB_389323), Brilliant Violet 605 anti-mouse CD4 (RM4-5, Biolegend, 0.33 µg/ml, 100548, AB_2563054), FITC anti-mouse CD4 (RM4-5, Biolegend, 5 µg/ml, 100510, AB_312712), APC anti-mouse CD8a (53-6.7, Biolegend, 0.5 µg/ml, 100712, AB_312751), Brilliant Violet 421 anti-mouse CD8a (53-6.7, Biolegend, 2 µg/ml, 100737, AB_10897101), PE/Cyanine7 anti-mouse CD11b (M1/70, Biolegend, 0.5 µg/ml, 101216, AB_312799), APC/Cyanine7 anti-mouse CD11b (M1/70, Biolegend, 2 µg/ml, 101226, AB_830641), PE anti-mouse CD11c (HL3, BD Bioscience, 0.5 µg/ml, 553802, AB_396684), PerCP anti-mouse CD45 (30-F11, Biolegend, 2 µg/ml, 103130, AB_893339), Brilliant Violet 605 anti-mouse CD45 (30-F11, Biolegend, 2 µg/ml, 103139, AB_2562341), PerCP anti-mouse CD45.2 (104, Biolegend, 2 µg/ml, 109826, AB_893349), Brilliant Violet 421 anti-mouse CD45R/B220 (RA3-6B2, Biolegend, 0.1 µg/ml, 103239, AB_10933424), PE anti-mouse CD45R/B220 (RA3-6B2, Biolegend, 2 µg/ml, 103208, AB_312992), APC/Cyanine7 anti-mouse Ly-6G/Ly-6C (RB6-8C5, Biolegend, 2 µg/ml, 108424, AB_2137485). Staining was done in 50 µl FACS Buffer at 4 °C for 20 min. Cells were washed and incubated for 10 min in 500 µl BD FACS™ Lysing solution (BD Bioscience, 349202) at room temperature. The lysis was stopped by the addition of FACS Buffer and the cells washed once before acquisition on a LSR Fortessa Flow Cytometer on a Beckmann-Coulter Cytoflex S.

Quantification of fecal lipocalin-2

Fecal pellets were processed as described above. Homogenized feces was centrifuged at 16000x *g* for 5 min and the resulting supernatant was analysed in duplicates using the mouse lipocalin-2 ELISA duoset (R&D, DY1857) according to the manufacturer's instructions.

Analysis of specific antibody titres by bacterial flow cytometry

Specific antibody titres in mouse intestinal washes and serum were measured by flow cytometry as described (*57*). Briefly, intestinal washes and blood were collected as described above. Blood was centrifuged at 10000x *g* for 5 min to obtain serum, heat-inactivated at 56 °C for 30 min and stored at -20 °C until further analysis. Intestinal lavage was centrifuged at 16000x *g* for 5 min to clear all bacterial-sized particles and stored at -20 °C until analysis. Bacterial targets (antigen against which antibodies are to be titred) were grown overnight in LB, then gently pelleted for 2 min at 7000x *g*. The pellet was washed with 0.2 µm-filtered PBS before resuspending at a density of approximately 10^7 bacteria per ml. After thawing, intestinal washes were centrifuged again at 16000x *g* for 5 min. Supernatants were used to perform serial dilutions. 50 µl of the dilutions were incubated with 50 µl bacterial suspension for 15 min at room temperature. Bacteria were washed twice with 150 µl PBS by centrifugation at 7000x *g* for 5 min, before resuspending in 25 µl of 0.2 µm-filtered PBS containing polyclonal Alexa Fluor 647 Rabbit Anti-Mouse IgG (Jackson ImmunoResearch, 15 µg/ml, 315-605-003, AB_2340239) or monoclonal Brilliant Violet 421 Rat Anti-Mouse IgA (BD Bioscience, 2 µg/ml, 743293,

AB_2741405). After 5 min of incubation at RT, bacteria were washed twice with PBS as above and resuspended in 100 µl PBS for acquisition on a Beckman Coulter Cytoflex S using FSC and SSC parameters to threshold acquisition in logarithmic mode. Data were analysed using FlowJo (Treestar). After gating on bacterial particles, log-median fluorescence intensities (MFI) were plotted against lavage dilution factor for each sample and 4-parameter logistic curves were fitted using Prism (Graphpad, USA). Titers were calculated from these curves as the dilution factor giving an above-background signal (typically MFI=300).

Histological procedures

Tissue embedded in OCT Compound was cut into 5 µm cryosections and mounted on glass slides. Cryosections were air dried overnight at room temperature and stained with hematoxylin and eosin (H&E). Scoring of cecal inflammation was done in a blinded manner assessing the following four criteria as previously described (*48*).

(i) Submucosal edema. Submucosal edema was scored as follows: 0 = no pathological changes; 1 = mild edema (the submucosa accounts for <50% of the diameter of the entire intestinal wall - tunica muscularis to epithelium); 2 = moderate edema (the submucosa accounts for 50 to 80% of the diameter of the entire intestinal wall); and 3 = profound edema (the submucosa accounts for >80% of the diameter of the entire intestinal wall).

(ii) PMN infiltration into the lamina propria. Polymorphonuclear granulocytes (PMN) in the lamina propria were enumerated in 10 high-power fields (x400 magnification; field diameter of 420 µm), and the average number of PMN/high-power field was calculated. The scores were defined as follows: 0 = <5 PMN/high-power field; 1 = 5 to 20 PMN/high-power field; 2 = 21 to 60/high-power field; 3 = 61 to 100/high-power field; and 4 = >100/high-power field. Transmigration of PMN into the intestinal lumen was consistently observed when the number of PMN was >60 PMN/high-power field.

(iii) Goblet cells. The average number of goblet cells per high-power field (magnification, x400) was determined from 10 different regions of the cecal epithelium. Scoring was as follows: 0 = >28 goblet cells/high-power field; 1 = 11 to 28 goblet cells/high-power field; 2 = 1 to 10 goblet cells/high-power field; and 3 = <1 goblet cell/high-power field.

(iv) Epithelial integrity. Epithelial integrity was scored as follows: 0 = no pathological changes detectable in 10 high-power fields (x400 magnification); 1 = epithelial desquamation; 2 = erosion of the epithelial surface (gaps of 1 to 10 epithelial cells/lesion); and 3 = epithelial ulceration (gaps of >10 epithelial cells/lesion; at this stage, there is generally granulation tissue below the epithelium). The combined pathological score for each tissue sample was determined as the sum of these scores. It ranges between 0 and 13 arbitrary units and covers the following levels of inflammation: 0 = intestine intact without any signs of inflammation; 1 to 2 = minimal signs of inflammation (this was frequently found in the ceca of SPF mice; this level of inflammation is generally not considered as a sign of disease); 3 to 4 = slight inflammation; 5 to 8 = moderate inflammation; and 9 to13 = profound inflammation.

Estimation of *in vivo* growth rates in the gut by plasmid dilution

Absolute *S*.Tm growth rates in the gut were assessed using replication-incompetent plasmid pAM34, which has been described previously(*7, 11*). Briefly, pAM34 is a ColE1-like vector in which the replication of the plasmid is under the control of the LacI repressor, whereby plasmid replication only occurs in the presence of isopropyl β-d-1-thiogalactopyranoside (IPTG). *S*.Tm carrying the pAM34 plasmid was therefore cultured overnight in the presence of 1 mM IPTG in LB containing streptomycin.

Cultures were diluted 1:20 into fresh LB broth without IPTG or antibiotics and sub-cultured for 3 h at 37 °C. Inocula for infections were prepared as described above. Concurrently, the inoculum was serially diluted into fresh LB broth without IPTG and cultured for 20 h at 37 °C to generate a standard curve relating plasmid loss to generations undergone for each experiment. pAM34-carrying bacteria within the overnight cultures and the feces were determined by selective plating on agar plates containing 50 µg/ml ampicillin and 1 mM IPTG. To quantify the total population size, samples were further plated on agar plates containing 100 µg/ml streptomycin. The fraction of pAM34-carrying bacteria was calculated using the ratio of pAM34-carrying CFU to the total population CFU and generations estimated by interpolation from the matched standard curve.

Non-typhoidal *Salmonella* transmission

Donor mice were vaccinated with PA-*S.*Tm as described above, orally pretreated with 25 mg streptomycin, and colonized 24 h later with $5{\cdot}10^3$ *S.*Tm^{Comp}. 2 days later, mice were treated again with 25 mg Streptomycin by orogastric gavage, and 24 h later infected with $1{\cdot}10^6$ *S.*Tm^{WT}. On day 9 post infection, one fecal pellet was collected from each mouse, weighed, and homogenized in 200 µl PBS. Large debris was removed by centrifugation at 500x *g* for 1 minute and 50 µl of the supernatant were immediately given by oral gavage to streptomycin pretreated naïve recipient mice. As a control, the same procedure was done using naïve mice without competitor colonization as donor mice. Recipient mice were euthanized, and organs were collected on day 3 post transmission. In both donor and recipient mice, fecal pellets were collected daily and selective plating was used to enumerate *Salmonella* and determine the relative proportions of both competing bacterial strains.

Flow cytometry for analysis of O:5 and O:12-0 intensity on *Salmonella* clonal cultures

Overnight cultures (1 µl) made in 0.2 µm-filtered lysogeny broth was stained with 0.2 µm-filtered solutions of STA5 (human recombinant monoclonal IgG2 anti-O:12-0, 3.2 µg/ml) (*7*) or rabbit anti-Salmonella O:5 (Difco, 1:200, 226601). After incubation at 4 °C for 30 min, the bacteria were washed twice by centrifugation at 7000x *g* and resuspension in PBS/2% BSA. The bacteria were then resuspended in 0.2 µm-filtered solutions of appropriate secondary reagents (Alexa 647-anti-human IgG (Jackson ImmunoResearch, 1:100, 109-605-098, AB_2337889) and Brilliant Violet 421-anti-rabbit IgG (BioLegend, 1:100, 406410, AB_10897810)). This was incubated for 30 min at 4 °C before the cells were washed as above and resuspended for acquisition on a Beckman Coulter Cytoflex S.

Statistical analysis

Sample size was determined based on previous experiments (*7, 10*). Where large effect sizes where expected a minimum of five mice/group were used. Researchers were not blinded for the assignment of the experiments and the data analysis except for histopathological scoring. Where errors are expected to be log-normal distributed (e.g., CFU determination or ELISA data based on serial dilutions), all statistical tests were carried out on log normalized data. Where two groups of data were compared, analysis was carried out using unpaired two-tailed t-test. One-way ANOVA followed by Tukey's Test was used for comparison of three or more groups. Statistical analysis on time course data was either done by mixed-effects analysis or by calculating the area under the curve (AUC) of the log normalized data and then assessing differences in AUC with one-way ANOVA and Tukey's test or false discovery rate (FDR) using the Benjamini–Hochberg procedure with alpha set to 0.05 or two-way ANOVA followed by Šídák's multiple comparisons test. Statistical analysis was performed with

Graphpad Prism Version 9.2.0 for Windows (GraphPad Software, La Jolla, California USA). P values of less than 0.05 are reported.

Supplementary Figures 1-12

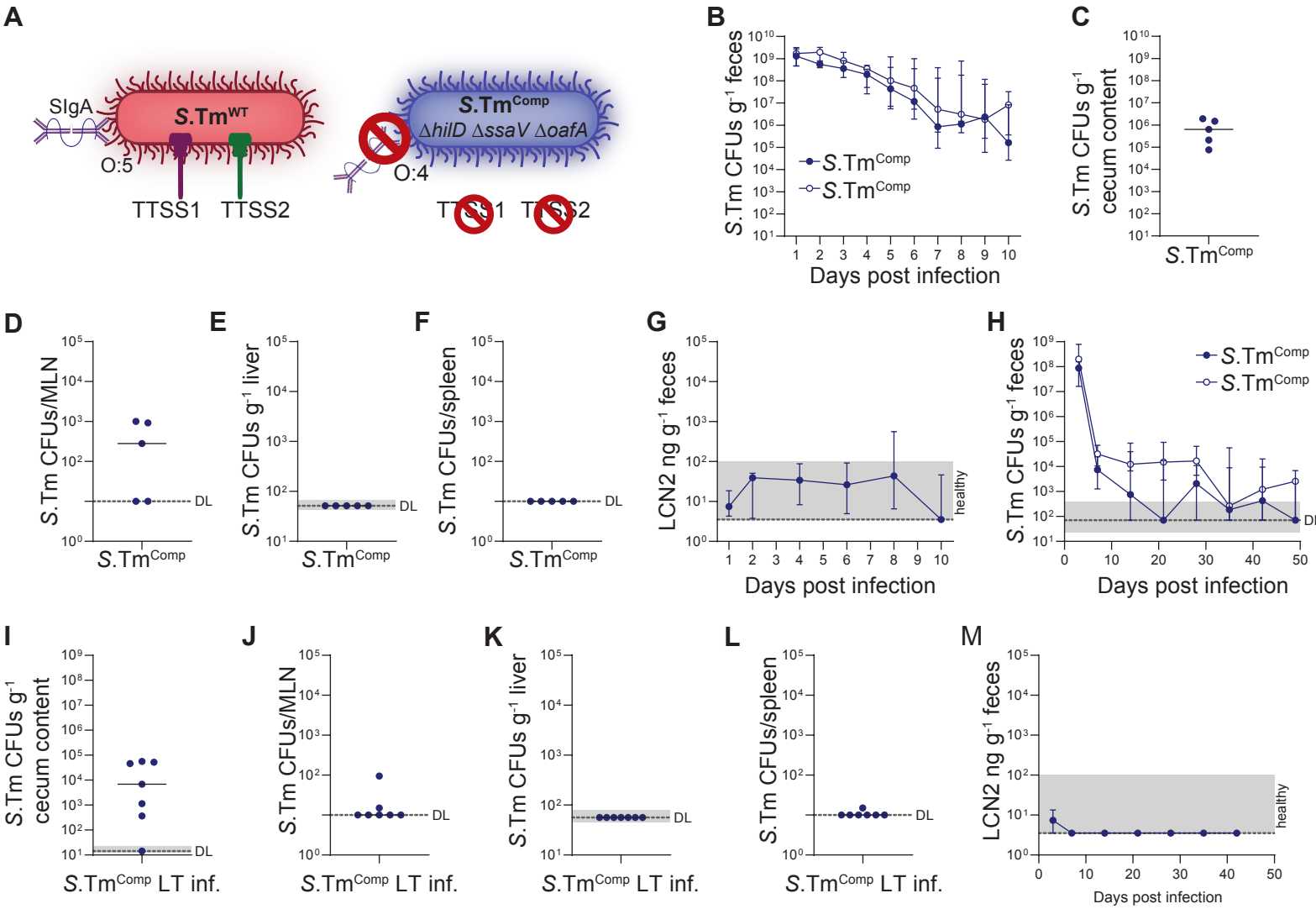

Figure S1. *S.*Tm^{Comp} is not pathogenic in 129S6/SvEv and C57BL/6J mice.

Figure S1. *S*.Tm^{Comp} is not pathogenic in 129S6/SvEv and C57BL/6J mice. (**A**) Schematic depiction of the introduced mutations rendering *S*.Tm^{Comp} non-pathogenic and preventing vaccine-induced IgA to bind. The expression of the type 3 secretion system (T3SS)-1 and T3SS-2 were inactivated by deletion of the genes encoding the master regulator *HilD* and an essential component of T3SS-2 *ssaV*, respectively. Around a third of the S.Tm population in an infection will not express T3SS-1 enabling faster growth, while still profiting from T3SS-1 induced inflammation from the rest of the population. SPI-2 will enable intracellular replication during invasive infection. To reduce IgA binding induced by vaccination with *S*.Tm^{WT}, the acetylation of abequose was prevented by deletion of *oafA*, generating an O:4,12 serovar. (**B-F**) 129S6/SvEv mice were pretreated with streptomycin and colonized with a total of 10^5 of a 1:1 mixture of two isogenic *S*.Tm^{Comp} strains and colonization was followed for 10 days. *S*.Tm^{Comp} strains differed only in their antibiotic resistance. *S*.Tm^{Comp} CFUs were determined by selective plating in feces (**A**) cecum content (**B**), MLN (**C**), liver (**D**) and spleen (**E**). Low numbers of live apathogenic bacteria are expected to be found in MLNs due to active sampling of luminal bacteria. (**F**) Intestinal inflammation was determined by measuring fecal lipocalin-2. (**G-L**) Mice of the highly susceptible (due to the lack of Nramp1) C57BL/6 strain were pretreated with streptomycin and infected with a total of 10^4 of a 1:1 mixture of two isogenic *S*.Tm^{Comp} strains and colonization was followed long-term for a total of 7 weeks. *S*.Tm^{Comp} CFUs were determined by selective plating in feces (**G**) cecum content (**H**), MLN (**I**), liver (**J**) and spleen (**K**). (**L**) Intestinal inflammation was determined by measuring fecal lipocalin-2. Taken together, the absence of systemic *S*.Tm^{Comp} counts and intestinal inflammation in Nramp1$^{+/+}$ and Nramp1$^{-/-}$ mice even upon long-term colonization confirms the avirulence of the designed *S*.Tm competitor.

N = 5-7 mice. Solid lines depict the median, error bars the interquartile range. Dotted lines show the detection limit and the shaded area the range for cases in which the detection limit is dependent on sample weight. Statistics were performed by an unpaired two-tailed t-test on log-normalized area under the curve (AUC) (A, G). CFU, colony forming unit; LCN2, lipocalin-2; MLN, mesenteric lymph node.

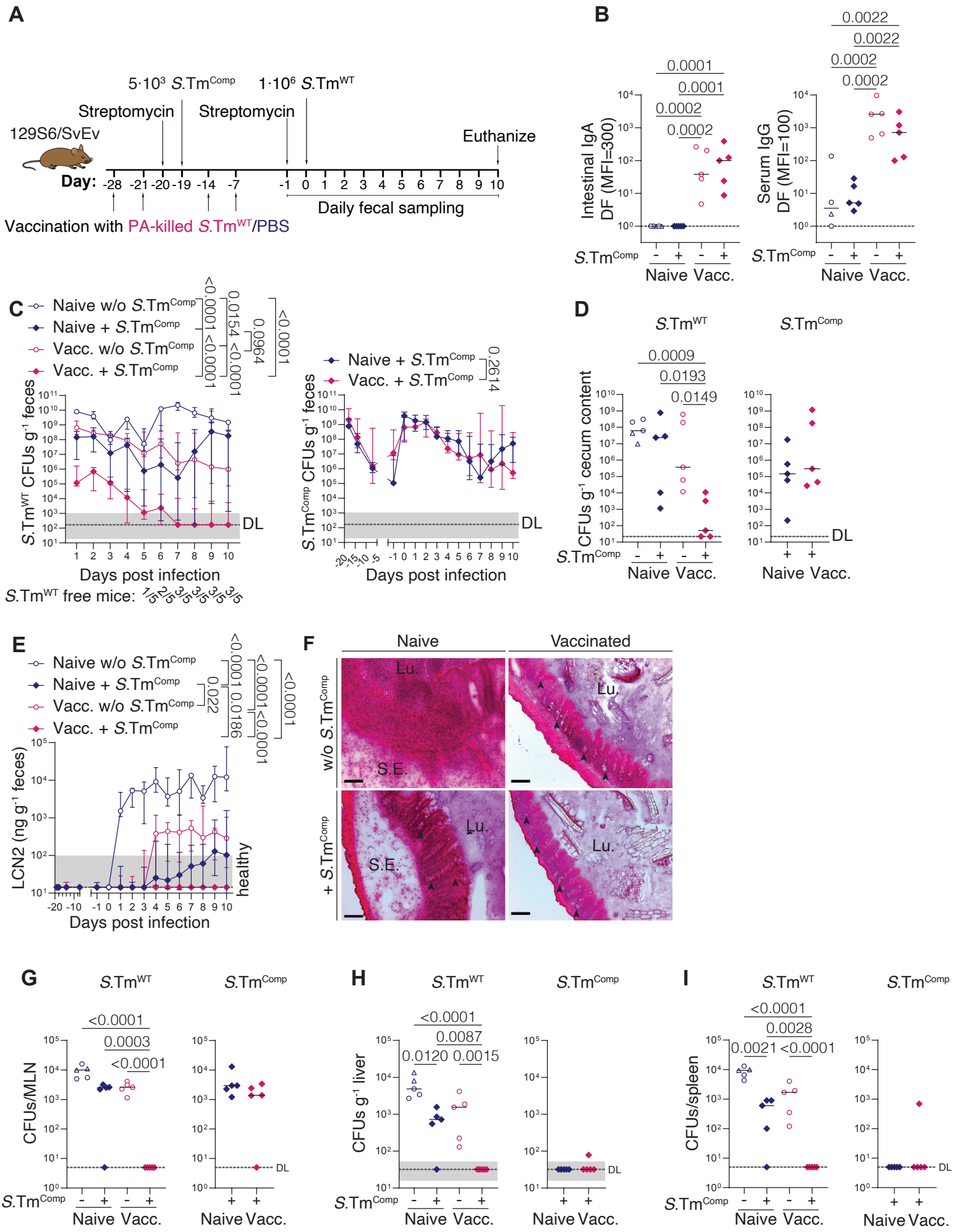

Figure S2. Vaccine-enhanced competition protects independently of the timepoint of *S.*Tm^{Comp} administration.

Figure S2. Vaccination-enhanced competition protects independent of the timepoint of *S*.Tm^{Comp} administration. The generated mathematical model, based on *in vivo* competition data, predicted that timing of competitor introduction would not change the outcome on *S*.Tm^{WT} clearance as long as the competitor was still present at the time of challenge. As *S*.Tm^{Comp} persisted in the intestine for several weeks, we decided to challenge PBS (blue symbols) or PA-*S*.Tm-vaccinated (pink symbols) streptomycin-pretretated 129S6/SvEv mice with $1{\cdot}10^6$ *S*.Tm^{WT} 19 days after receiving $5{\cdot}10^3$ *S*.Tm^{Comp}. This timing would be feasible, for example, for pre-travel prophylaxis. (**A**) Experimental procedure. (**B**) *S*.Tm^{WT}-specific intestinal IgA and serum IgG titres at 10 days post infection as determined by flow cytometry. Fecal (**C**) and cecum content (**D**) *S*.Tm CFUs as determined by selective plating. (**E**) Intestinal inflammation as determined by fecal lipocalin. (**F**) Representative images of H&E-stained cecal tissue sections. Arrowheads show exemplary goblet cells. Scale bars: 100 µm. (**G-I**) *S*.Tm CFUs in MLN (**G**), liver (**H**) and spleen (**I**).

N = 5 mice/group. Solid lines depict the median, error bars the interquartile range. Dotted lines show the detection limit and the shaded area the range for cases in which the detection limit is dependent on sample weight. Open triangles show mice (n = 2) that had to be euthanized prematurely due to excessive weight loss (≥ 15%) or disease symptoms. Statistics were performed by one-way ANOVA on log-normalized data (B, D, G-I) or area under the curve (AUC) (C, E). Where only two groups were compared, an unpaired two-tailed t-test on log-normalized data was done (D, G-I). CFU, colony forming unit; LCN2, lipocalin-2; Lu., lumen; MFI, median fluorescence intensity; MLN, mesenteric lymph node; S.E., submucosal edema.

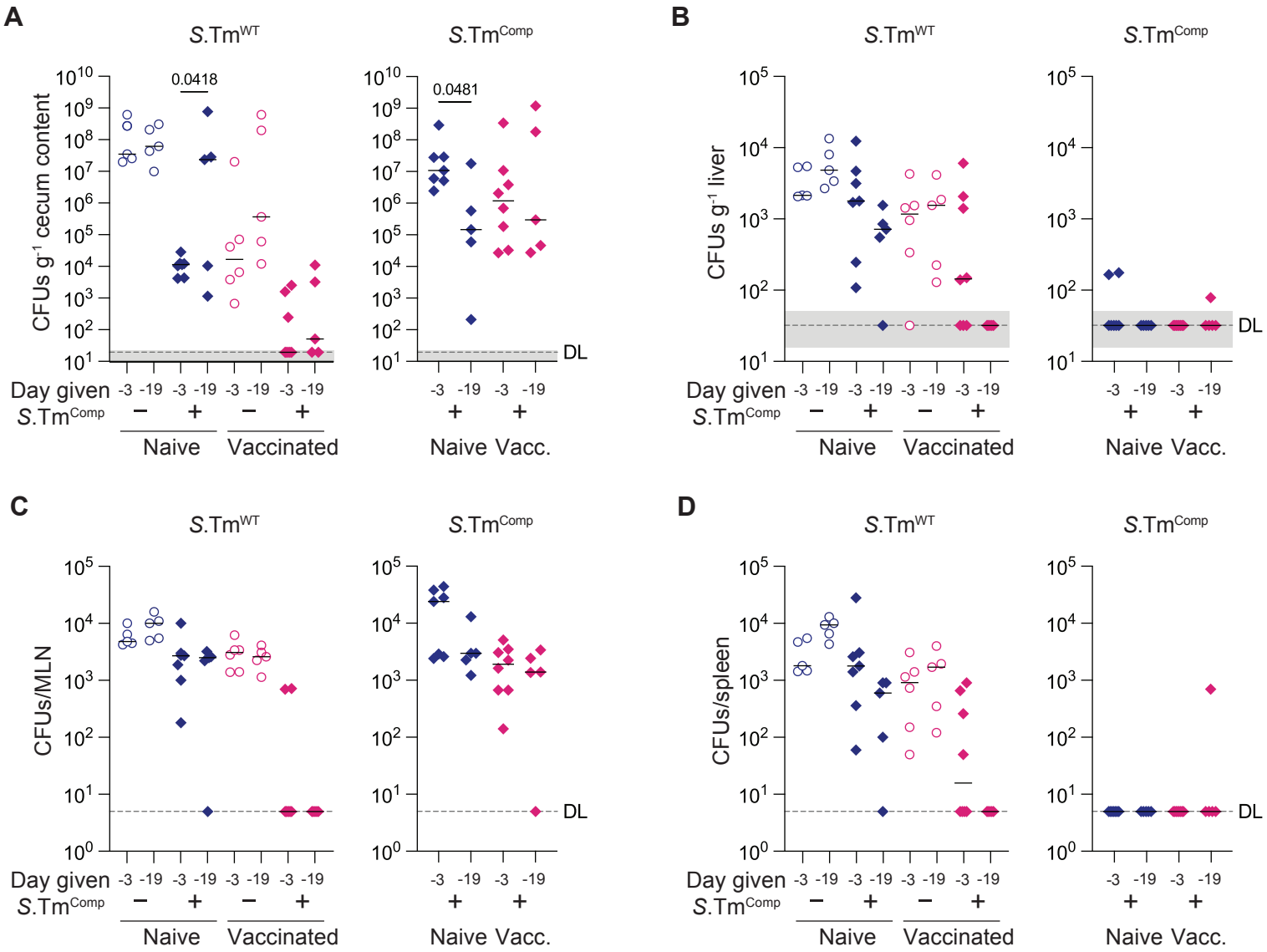

Figure S3. Timing of *S*.Tm^{Comp} pre-colonization does not influence the efficacy of vaccine-enhanced competition.

Figure S3. Timing of *S*.Tm^{Comp} pre-colonization does not influence the efficacy of vaccine-enhanced competition. Endpoint data from Fig. 1 and fig. S2. PBS or PA-*S*.Tm-vaccinated 129S6/SvEv mice were pre-colonized with $5 \cdot 10^3$ *S*.Tm^{Comp} either 3 or 19 days prior to infection with $1 \cdot 10^6$ *S*.Tm^{WT}. *S*.Tm CFUs in cecum content (**A**), liver (**B**), MLN (**C**) and spleen (**D**).

Pooled data from three independent experiments (n = 5-8 mice/group). Solid lines depict the median. Dotted lines show the detection limit and the shaded area the range for cases in which the detection limit is dependent on sample weight. Statistics were performed by one-way ANOVA on log-normalized data.

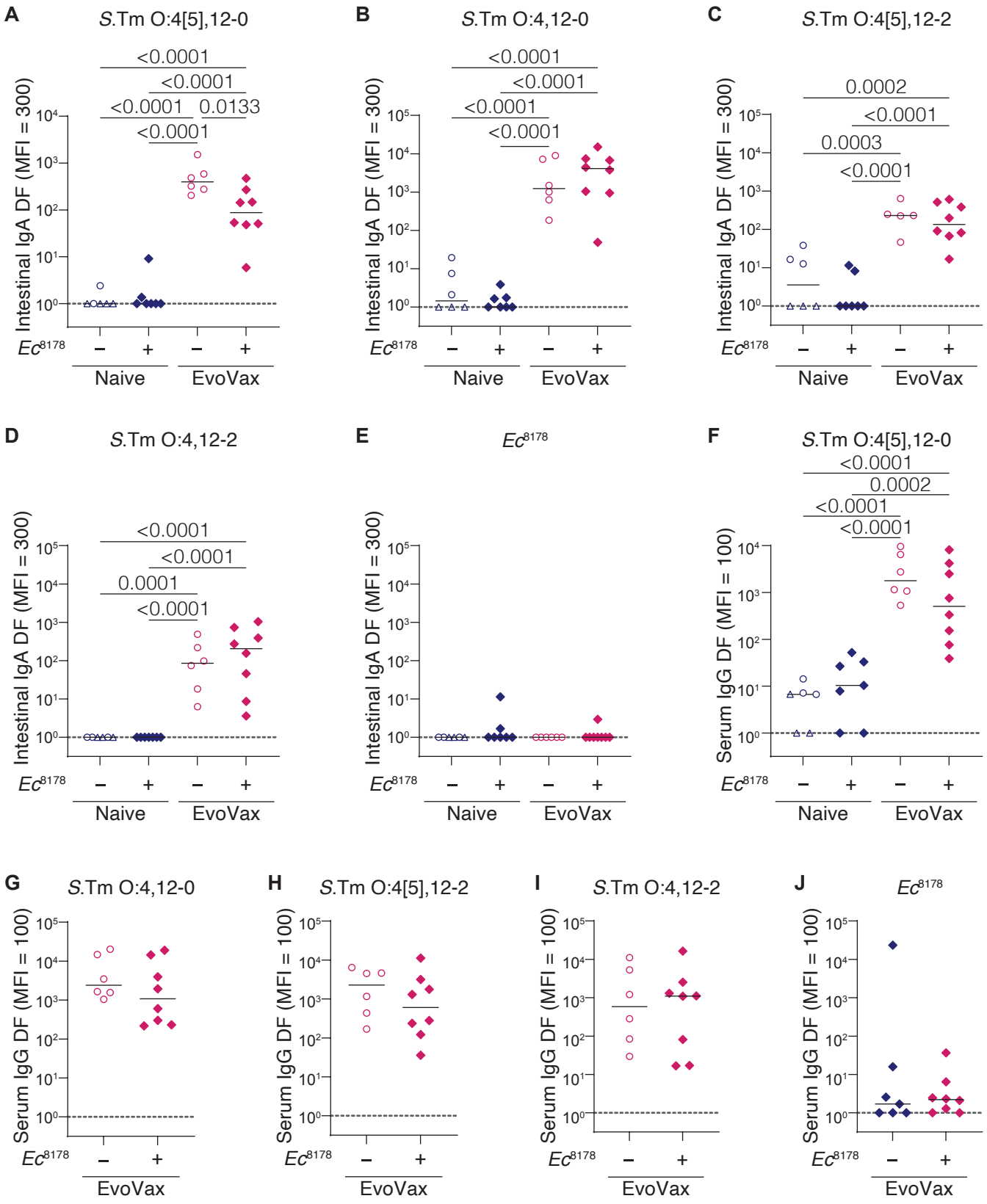

Figure S4. Vaccination with EvoVax generates an intestinal IgA and serum IgG response against all *S*.Tm O-antigen variants but not the competitor strain *E. coli* 8178.

Figure S4. Vaccination with EvoVax generates an intestinal IgA and serum IgG response against all *S*.Tm O-antigen variants but not the competitor strain *E. coli* 8178. The "evolutionary trap" version of our *S*.Tm vaccine, consisting of all possible O-antigen variants of *S*.Tm, induces an IgA response that rapidly selects for loss of the polymerized O-antigen, and correspondingly for attenuation of *S.*Tm *(10)*. Therefore, we here combine a more powerful inactivated oral vaccine with a less ideal (but safer) niche competitor, which is not recognized by induced antibodies.

129S6/SvEv mice were mock-vaccinated with PBS (blue symbols) or EvoVax vaccinated (pink symbols) and later infected with $1{\cdot}10^6$ *S*.Tm^{WT} with or without pre-colonization with $5{\cdot}10^3$ *E. coli* 8178. 10 days after *S*.Tm^{WT} infection, *S*.Tm- and *E.* coli 8178-specific antibody responses were determined in intestinal lavage (**A-E**) and serum (**F-J**) by flow cytometry. (**A+F**) *S*.Tm O:4[5],12-0. (**B+G**) *S*.Tm O:4,12-0. (**C+H**) *S*.Tm O:4[5],12-2. (**D+I**) *S*.Tm O:4,12-2. (**E+J**) *E.* coli 8178.

Pooled data from two independent experiments (n = 6-8 mice/group). Solid lines depict the median. Dotted lines show the detection limit. Open triangles show mice that had to be euthanized prematurely due to excessive weight loss (≥ 15%) or disease symptoms. Statistics were performed one-way ANOVA on log-normalized data and Tukey's test (A-F). Where only two groups were compared, an unpaired two-tailed t-test on log-normalized data was done (G-J). DF, dilution factor; MFI, median fluorescence intensity.

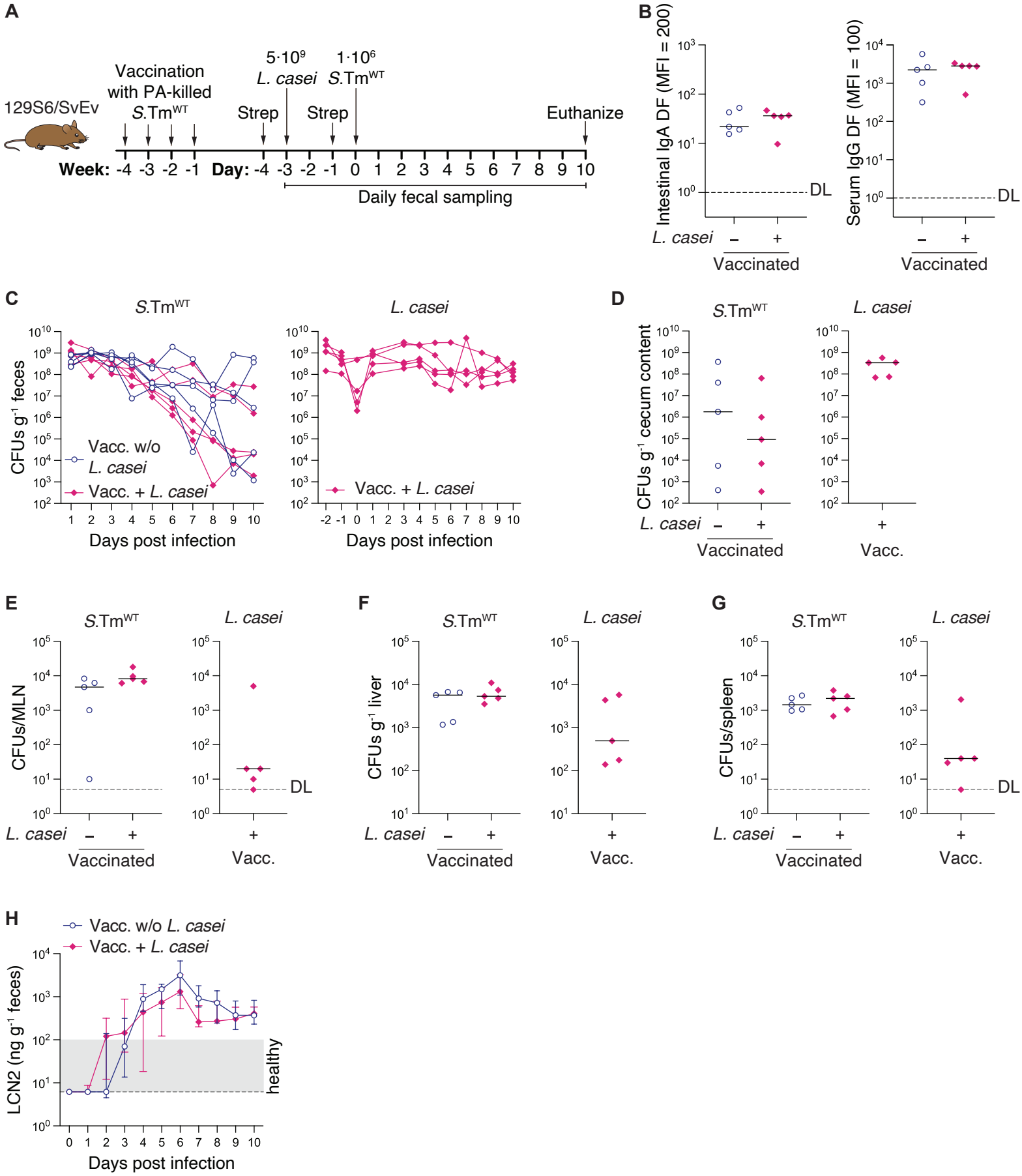

Figure S5. An unrelated probiotic strain does not improve *S*.Tm^{WT} clearance or intestinal inflammation on top of vaccination.

Figure S5. An unrelated probiotic strain does not improve *S*.Tm^{WT} clearance or intestinal inflammation on top of vaccination. *L. casei* has been demonstrated to enhance IgA production and immunological protection via enhanced innate immune functions *(23)*. The limited impact of L. casei in our experiments, suggests that these mechanisms are not major drivers of vaccine-enhanced competition in this model.

PBS or PA-*S*.Tm-vaccinated 129S6/SvEv mice were pre-colonized with with $5 \cdot 10^3$ *L. casei* and 3 days later infected with $1 \cdot 10^6$ *S*.Tm^{WT}. (**A**) Experimental procedure. (**B**) *S*.Tm^{WT}-specific intestinal IgA and serum IgG titres at 10 days post infection as determined by flow cytometry. CFUs in feces (**C**), cecum content (**D**), MLN (**E**), liver (**F**) and spleen (**G**) as determined by selective plating. (**H**) Intestinal inflammation as determined by fecal lipocalin.

N = 5 mice/group. Solid lines depict the median, error bars the interquartile range. Dotted lines show the detection limit and the shaded area the range for cases in which the detection limit is dependent on sample weight. Statistics were performed by one-way ANOVA on log-normalized data (B, D, E-G) or area under the curve (AUC) (C, H). Where only two groups were compared, an unpaired two-tailed t-test on log-normalized data was done (D, E-G). CFU, colony forming unit; LCN2, lipocalin-2; MFI, median fluorescence intensity; MLN, mesenteric lymph node.

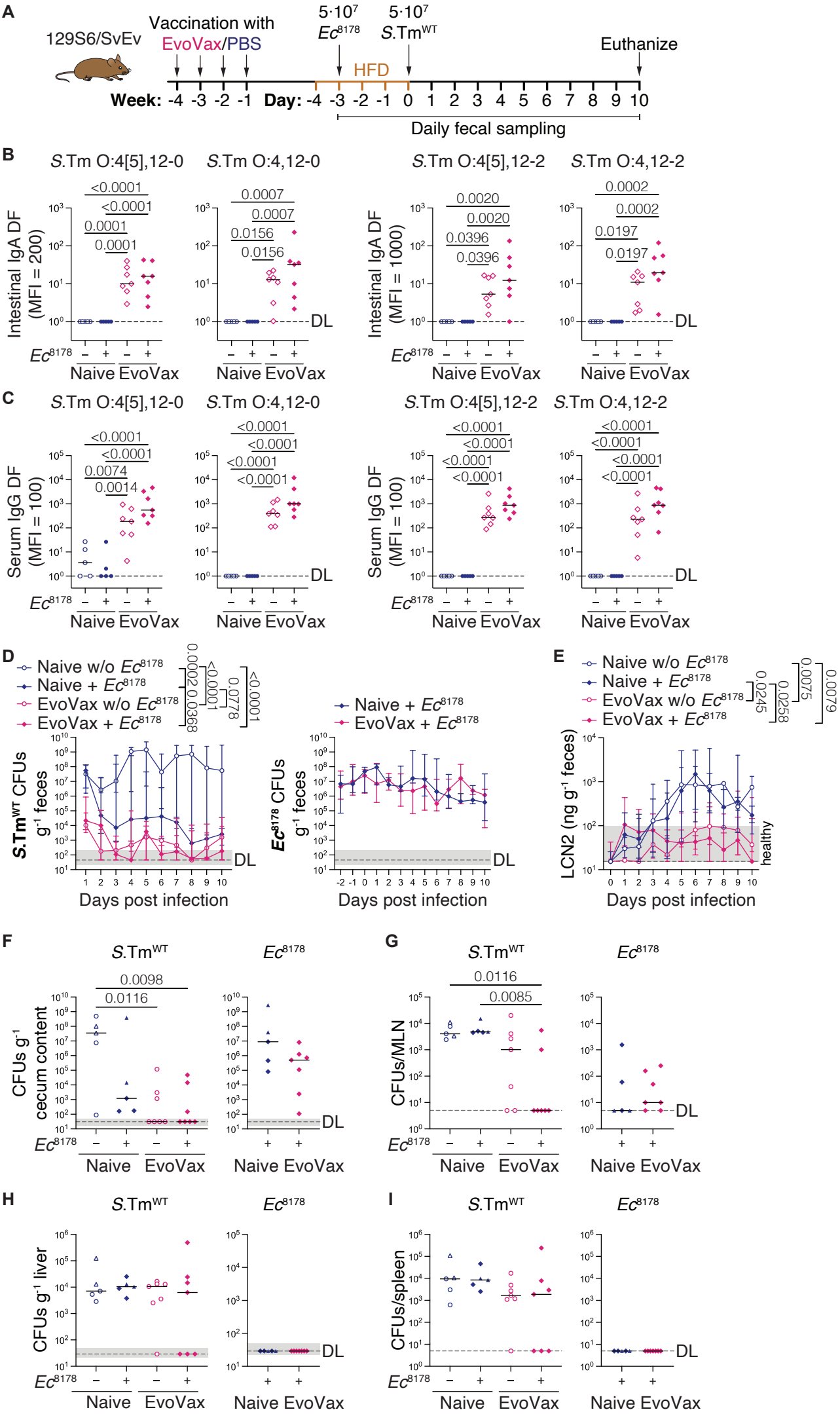

Figure S6. Vaccine-enhanced competition with an imperfect niche competitor is sufficient for protection in cases of less severe and transient microbiota disruptions.

Figure S6. Vaccine-enhanced competition with an imperfect niche competitor is sufficient for protection in cases of less severe and transient microbiota disruptions. As diet switches are common in human, especially when travelling, we wanted to test the protectiveness of vaccine-enhanced competition in a high-fat diet model. In comparison to antibiotic treatment, this causes only a mild microbiota disruption. Due to the decreased stringency of this model both oral vaccination alone and niche-competitor alone are effective in preventing *S*.Tm colonization but vaccine-enhanced competition shows slightly better protection from systemic spread. PBS or EvoVax vaccinated 129S6/SvEv mice were switched to a fibre-free high fat diet (HFD) for 4 days and infected with $5{\cdot}10^7$ *S*.Tm^{WT}. Two groups were pre-colonized with $5{\cdot}10^7$ *E. coli* 8178 3 days before infection. (**A**) Experimental procedure. Antibody responses were determined in intestinal lavage (**B**) and serum (**C**) against all *S*.Tm O-antigen variants by flow cytometry. (**D**) Fecal CFUs as determined by selective plating. (**E**) Intestinal inflammation as determined by fecal lipocalin. CFUs in cecum content (**F**), MLN (**G**), liver (**H**) and spleen (**I**).

N = 5-7 mice/group. Solid lines depict the median, error bars the interquartile range. Dotted lines show the detection limit and the shaded area the range for cases in which the detection limit is dependent on sample weight. Statistics were performed by one-way ANOVA on log-normalized data (B-C, F-I) or area under the curve (AUC) (D-E). Where only two groups were compared, an unpaired two-tailed t-test on log-normalized data was done (F-I). CFU, colony forming unit; LCN2, lipocalin-2; MFI, median fluorescence intensity; MLN, mesenteric lymph node.

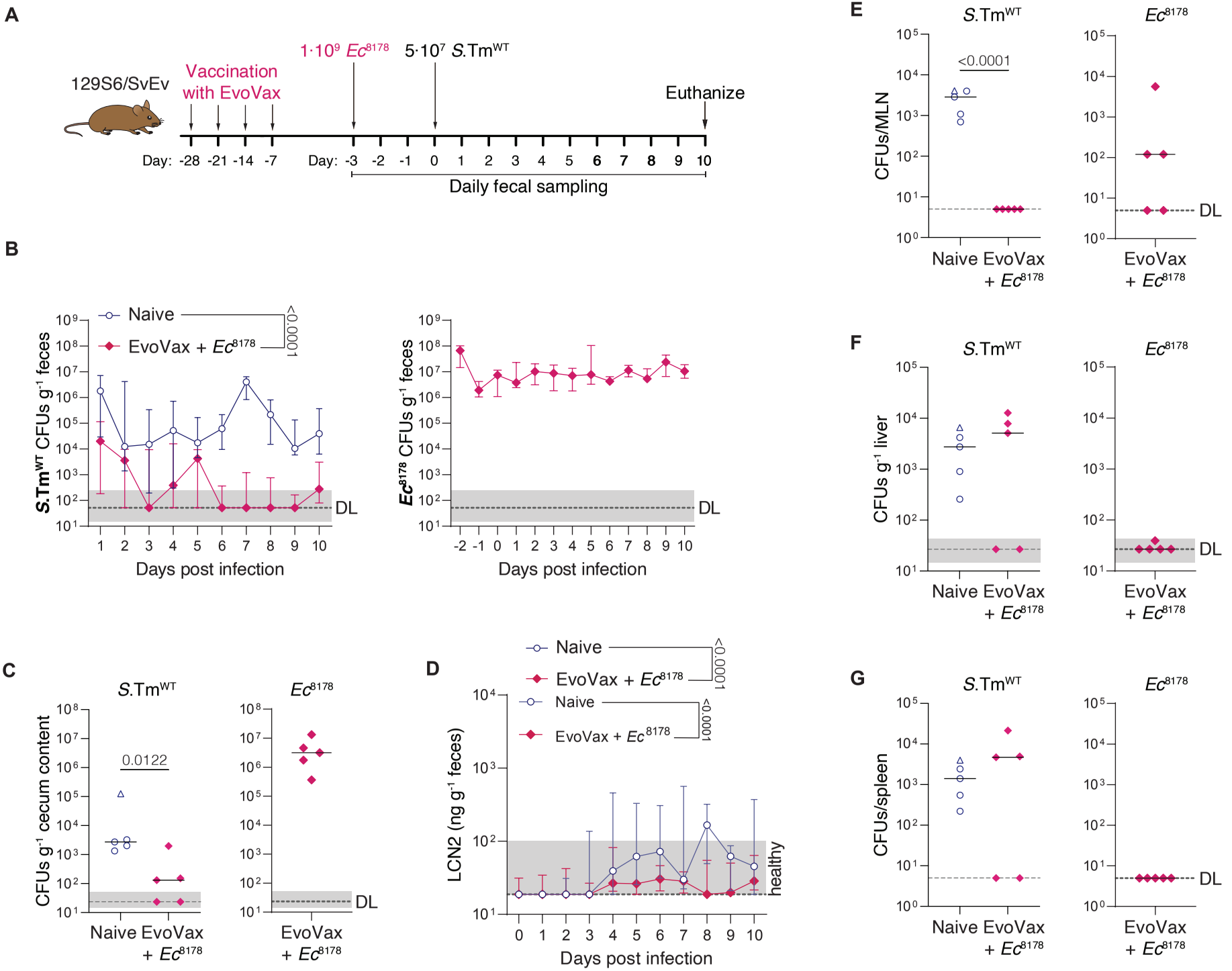

Figure S7. Vaccine-enhanced competition protects against intestinal pathology but not systemic invasion of *S*.Tm^{WT} in the murine Typhi model.

Figure S7. Vaccine-enhanced competition protects better against intestinal pathology but not systemic invasion of *S*.Tm^{WT} in the murine Typhi model. To benchmark vaccine-enhanced competition, we tested it in the murine oral typhoid model, i.e. a high-dose oral challenge without antibiotic pre-treatment. Vaccine-enhanced competition could prevent intestinal colonization and supress any detectable increase in intestinal lipocalin-2 levels.

PBS (blue circles) or EvoVax + *Ec*^{8178} (pink diamonds) 129S6/SvEv mice were infected with $5{\cdot}10^7$ *S*.Tm^{WT} without antibiotic pretreatment. EvoVax vaccinated mice were pre-colonized with $1{\cdot}10^9$ *E. coli* 8178 3 days before infection. (**A**) Experimental procedure. Fecal **(B)** and cecum content (**C**) CFUs as determined by selective plating. (**D**) Intestinal inflammation as determined by fecal lipocalin-2. (**E-G**) CFUs in MLN (**E**), liver (**F**) and spleen (**G**).

N = 5 mice/group. Solid lines depict the median, error bars the interquartile range. Dotted lines show the detection limit and the shaded area the range for cases in which the detection limit is dependent on sample weight. Open triangles show mice that had to be euthanized prematurely due to excessive weight loss (≥ 15%) or disease symptoms (n = 1).

Statistics were performed by one-way ANOVA on log-normalized data (C, E-G) or area under the curve (AUC) (B, D). CFU, colony forming unit; LCN2, lipocalin-2; MLN, mesenteric lymph node.

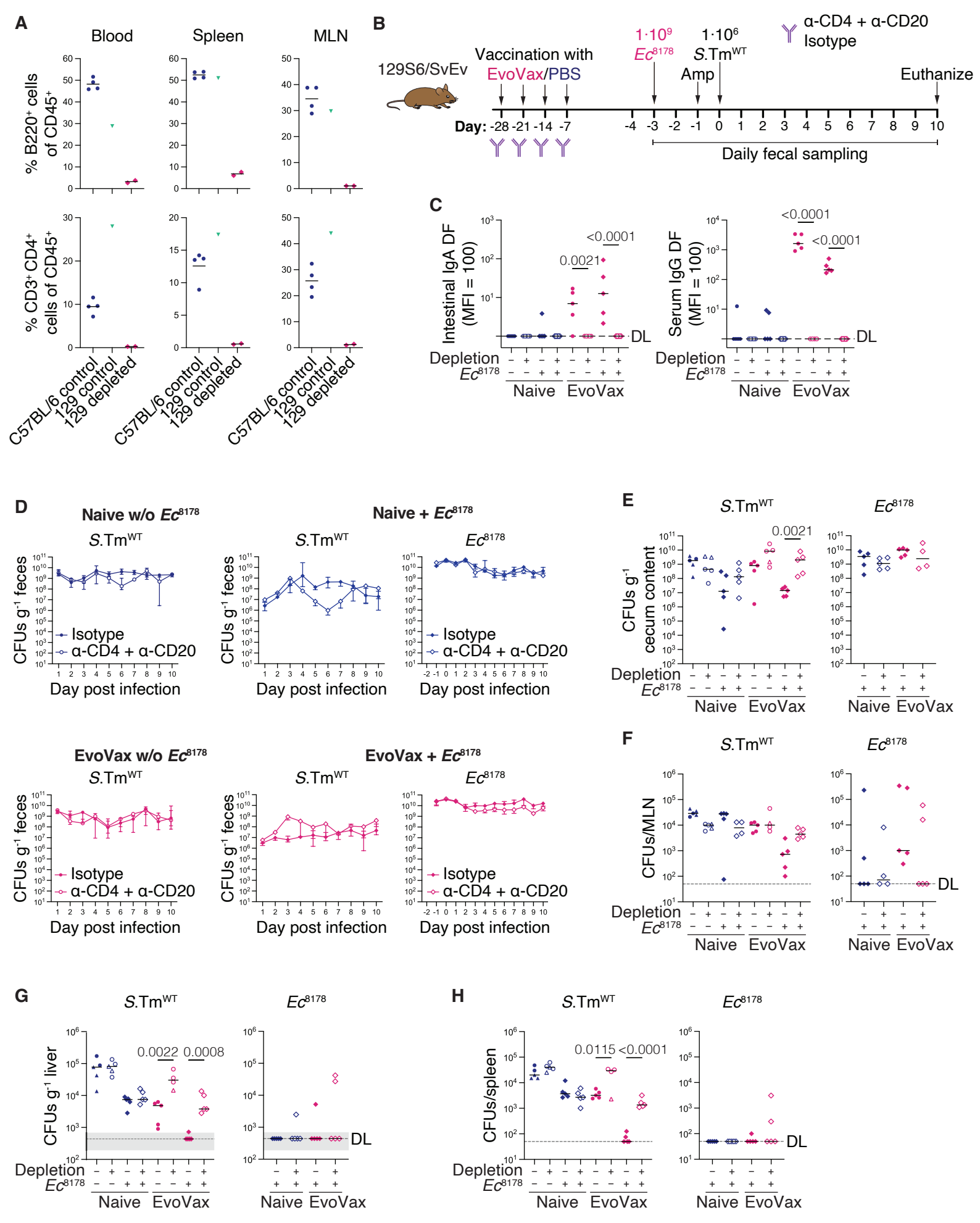

Figure S8. Antibodies are an integral part of protection in vaccine-enhanced competition.

Figure S8. Antibodies are an integral part of protection in vaccine-enhanced competition. As it has been reported that initial suppression of *Salmonella* growth is mediated by non-specific innate immune mechanisms *(29)*, we depleted both B cells and $CD4^+$ T cells in our vaccine-enhanced competition model. This showed that vaccine-induced antibodies limited initial *S*.Tm^{WT} expansion and systemic spread.

(**A**) Frequency of B cells and $CD4^+$ T cells among $CD45^+$ cells in depleted 129S6/SvEv (129 depleted) or control 129S6/SvEv (129 control) and C57BL/6 mice were measured in blood, spleen and MLNs by flow cytometry. Solid lines show the mean. (**B**) Experimental procedure. PBS (blue circles) or EvoVax vaccinated (pink diamonds) 129S6/SvEv mice were pretreated with ampicillin and infected with $1{\cdot}10^6$ *S*.Tm^{WT}. Some groups were pre-colonized with $1{\cdot}10^9$ *E. coli* 8178 3 days before infection as indicated. Mice were treated with anti-CD4 and anti-CD20 or isotype control one day prior to every vaccination. (**C**) *S*.Tm^{WT}-specific antibody responses were determined in intestinal lavage and serum at endpoint. CFUs in feces (**D**), cecum content (**E**), MLN (**F**), liver (**G**) and spleen (**H**).
N = 5 mice/group. Solid lines depict the median unless stated otherwise, error bars the interquartile range. Dotted lines show the detection limit and the shaded area the range for cases in which the detection limit is dependent on sample weight. Open triangles show mice (n = 5) that had to be euthanized prematurely due to excessive weight loss (≥ 15%) or disease symptoms. Statistics were performed by one-way ANOVA on log-normalized data (C, E-G). CFU, colony forming unit; MLN, mesenteric lymph node.

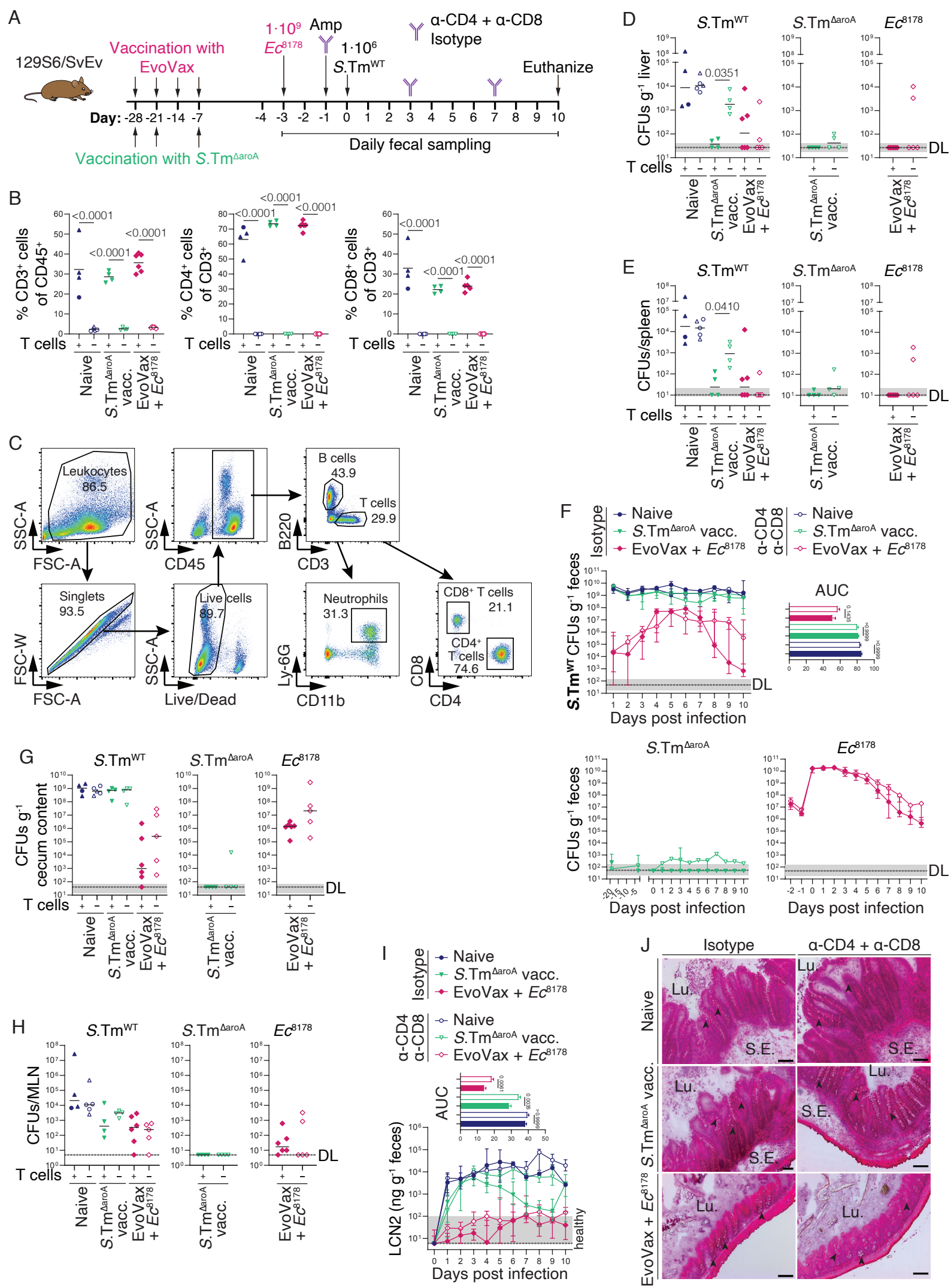

Figure S9. T cells mediate protection from invasive disease provided by live-attenuated vaccination but play only a minor role in protection provided by vaccine-enhanced competition.

Figure S9. T cells mediate protection from invasive disease provided by live-attenuated vaccination but play only a minor role in protection provided by vaccine-enhanced competition. The efficiency of vaccine-enhanced competition based on whole-cell inactivated oral vaccines prompted us to mechanistically compare this to live-attenuated Salmonella vaccines. In the non-Typhoidal Salmonellosis model, tissue invasion can be prevented either by sufficiently suppressing gut colonization levels *(22)*, or via effector T-cell mediated immunity *(24)*. Consistent with these vaccines relying predominantly on differing mechanisms, vaccine-enhanced competition, but not live-attenuated vaccines, dramatically reduced gut lumen colonization. Live-attenuated vaccines, but not whole-cell inactivated oral vaccines, provide T-cell mediated protection of deep tissues. Therefore vaccine-enhanced competition, based on whole-cell inactivated oral vaccines, functions predominantly by suppressing gut colonization and preventing initial tissue invasion, which protects both gut tissues and systemic sites, and prevents transmission. In contrast, live-attenuated vaccines provide protection of systemic sites despite strong gut colonization but very little protection of the gut tissues or impact on gut infectious reservoir.

PBS (blue circles), EvoVax vaccinated (pink diamonds) or *S*.Tm^{aroA} vaccinated (green triangles) 129S6/SvEv mice were pretreated with ampicillin and infected with $1{\cdot}10^6$ *S*.Tm^{WT}. EvoVax vaccinated mice were pre-colonized with $1{\cdot}10^9$ *E. coli* 8178 3 days before infection. Mice were treated with anti-CD4 and anti-CD8 or isotype control the day before infection, and then every fourth day. (**A**) Experimental procedure. (**B**) Frequency of T cells among CD45$^+$ cells in spleen. Frequency of CD4$^+$ and CD8$^+$ T cells among total T cells. Solid lines show the mean. (**C**) Gating strategy. CFUs in liver (**D**), spleen (**E**), feces (**F**), cecum content (**G**) and MLN (**H**). (**I**) Intestinal inflammation as determined by fecal lipocalin. (**J**) Representative images of H&E-stained cecal tissue sections. Arrowheads show exemplary goblet cells. Scale bars: 100 µm.

N = 4-6 mice/group. Solid lines depict the median unless stated otherwise, error bars the interquartile range. Dotted lines show the detection limit and the shaded area the range for cases in which the detection limit is dependent on sample weight. Open triangles show mice (n = 5) that had to be euthanized prematurely due to excessive weight loss (≥ 15%) or disease symptoms. Statistics were performed by one-way ANOVA (B) on log-normalized data (D-E, G-H) or area under the curve (AUC) (F, I). CFU, colony forming unit; LCN2, lipocalin-2; Lu., lumen; MLN, mesenteric lymph node; S.E., submucosal edema.

Supplementary Modelling text: Mathematical modeling of *S*.Tm^{WT} extinction in the gut

As competitive intestinal colonization is necessarily a highly dynamic process, we built a simple mathematical model to generate predictions of the requirements for extinction of *S*.Tm^{WT} from the gut lumen, and for the time-to-extinction. Based on previous quantification in the non-typhoidal Salmonella mouse model (*7, 17, 22, 26*), minimizing the time to extinction in the gut lumen should have three beneficial consequences:

1) By minimizing the duration and intensity of contact between wildtype *Salmonella* and host tissues, this minimizes the risk of *Salmonella* invasive disease.

2) By minimizing the number of wildtype *Salmonella* shed to the environment in feces, this minimizes the risk of transmission.

3) By minimizing the effective population size of wildtype *Salmonella*, this minimizes the risk of bacterial evolution of immune escape.

Of note, we do not attempt to model the influence of bacterial evolution on the outcome of vaccination, but based on our previous work (*10*) we expect that ignoring this parameter will lead to an overestimate of the efficacy of vaccination alone, and much less of an overestimate of the efficacy of vaccination plus niche competition.

In this model we assumed that the microbiota (of size M(t)), *S*.Tm^{Comp} (of size C(t)) and *S*.Tm^{WT} (of size W(t)) have access to three categories of resources that can be used for growth.

1) Undefined public resources, for which Salmonella, its competitor and the microbiota compete to contribute to the carrying capacity, K_1.

2) Undefined private resources that the microbiota cannot access, and *Salmonella* strains compete for, finally contributing to a carrying capacity K_2, i.e. in the absence of a competitor, wildtype *Salmonella* can colonize this niche long-term.

3) a private undefined resource for the microbiota that *Salmonella* cannot compete for, contributing to a carrying capacity K_3.

We assume that the two *Salmonella* strains and the microbiota have independent growth and clearance rates. This broadly represents the observation that avirulent *Salmonella* can colonize at a low density, long-term in mice from our SPF mouse colony.

In a deterministic view, the size of the populations evolves as

Eq. 1

$$\begin{cases} \frac{dW}{dt} = W \cdot \left(r_w \cdot \left(1 - \frac{1}{\frac{K_1}{M+C+W} + \frac{K_2}{C+W}} \right) - c_w \right) \\ \frac{dC}{dt} = C \cdot \left(r_c \cdot \left(1 - \frac{1}{\frac{K_1}{M+C+W} + \frac{K_2}{C+W}} \right) - c_c \right) \\ \frac{dM}{dt} = M \cdot \left(r_m \cdot \left(1 - \frac{1}{\frac{K_1}{M+C+W} + \frac{K_3}{M}} \right) - c_m \right) \end{cases}$$

where r_w, r_c and r_m correspond to the growth rate of *S*.Tm^{WT}, *S*.Tm^{Comp} and the microbiota, respectively. The parameters c_w, c_c and c_m correspond to the clearance rates of these populations.

In order to predict "extinction probability" and "extinction time", we required realistic estimates of the population dynamics of the two *S*.Tm strains and the "average microbiome". *S*.Tm growth and clearance rates in the presence or absence of IgA were estimated by fitting the obtained fecal CFU data for S.Tm^{WT} and S.Tm^{Comp} where both bacteria were administered simultaneously into vaccinated and naïve mice (Fig. S10A-C). The non-replicating plasmid, pAM34, was used to track generation numbers over the first 12 hours of infection to directly infer the number of generations starting from an inoculum of 1e4 or 1e6 *S*.Tm^{WT} (Fig. S10A and B). This confirmed the predicted slightly higher net growth rate for *S*.Tm^{Comp} as compared to *S*.Tm^{WT}. Integrating these numbers into the time-course of *S*.Tm^{WT} colonization also confirms the suppression of growth by the niche competitor and the elevated clearance rate of *S*.Tm^{WT} in vaccinated mice (see table S3).

r_w	r_c	r_m	
33.7 day^{-1}	38.7 day^{-1}	18.7 day^{-1}	
c_w	c_c	c_m	
6.4 day^{-1}	5.9 day^{-1}	1.7 day^{-1}	
K_1	K_2	K_3	m_0
$5.9 \cdot 10^9$	$2.3 \cdot 10^4$	10^7	10^5

Table S3. Kinetic parameter values inferred from direct competition data shown in fig. S10C below (for vaccinated + *S*.Tm^{Comp} group). r_w, r_c and r_m: growth rate of *S*.Tm^{WT}, *S*.Tm^{Comp} and the microbiota, respectively. c_w, c_c and c_m: clearance rates of *S*.Tm^{WT}, *S*.Tm^{Comp} and the microbiota. K_1, K_2, K_3: carrying capacities of *S*.Tm and the microbiota, *S*.Tm^{WT} and *S*.Tm^{Comp} and the microbiota alone. m_0: size of

microbiota after antibiotic clearance at time point of infection with *S*.Tm^{WT}. See section below for details.

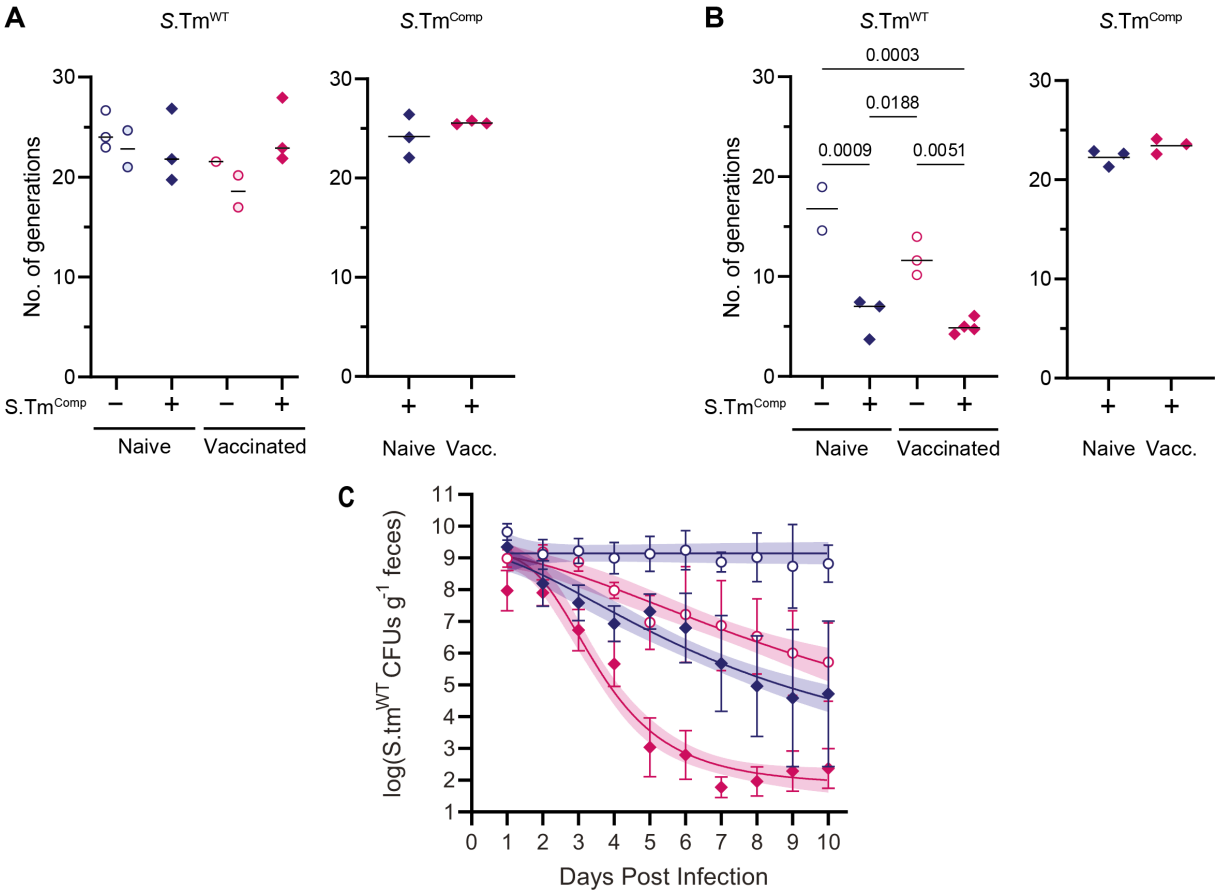

Fig. S10: Parameter estimation for *S*.Tm^{WT} extinction in the presence of vaccination and/or niche competition. (**A**) PBS (blue symbols) or PA-*S*.Tm-vaccinated (pink symbols) 129S6/SvEv mice were pretreated with streptomycin and co-infected with a total of 10^4 of a 1:1 mixture of two isogenic *S*.Tm^{WT} strains (circles) or *S*.Tm^{WT} and *S*.Tm^{Comp} (*S*.Tm$^{hilD\ ssaV\ oafA}$, filled diamonds). Number of generations 12 hours post infection was estimated based on the loss of pAM34. Open and filled circles show the two isogenic *S*.Tm^{WT} strains. (**B**) PBS (blue symbols) or PA-*S*.Tm-vaccinated (pink symbols) 129S6/SvEv mice were pretreated with streptomycin and infected with $1{\cdot}10^6$ *S*.Tm^{WT}. Two groups were pre-colonized with $5{\cdot}10^3$ *S*.Tm^{Comp} 3 days before infection. Number of generations 12 hours post infection was calculated based on the loss of pAM34. Solid lines depict the mean. Statistics were performed by one-way ANOVA. (**C**) PBS (blue symbols) or PA-*S*.Tm-vaccinated (pink symbols) 129S6/SvEv mice were pretreated with streptomycin and infected with a total of 10^4 of a 1:1 mixture of two isogenic *S*.Tm^{WT} strains (circles) or *S*.Tm^{WT} and *S*.Tm^{Comp} (*S*.Tm$^{hilD\ ssaV\ oafA}$, filled diamonds). Feces were collected over 10 days and CFU/g of *S*.Tm^{WT} calculated via plating.

For simplicity, all mathematical modelling was based on the arithmetic mean of the log-normalized experimental data, except if explicitly stated otherwise.

We consider a case where $K_2 \ll K_1$ because the height of final *S*.Tm^{Comp} "plateau" observed in competition data (which is proportional to K_2, see calculations below) is much lower than the size of *S*.Tm^{Comp} population at day 1 (which is proportional to K_1, see calculations below). We successively consider the cases $K_1 \ll K_3$ and $K_3 \ll K_1$ and conclude that the latter is more compatible with the

competition data. In the competition data (vaccinated group with *S*.Tm^{Comp}), several distinct regimes can be observed (fig. S11), which are also highlighted below with the model.

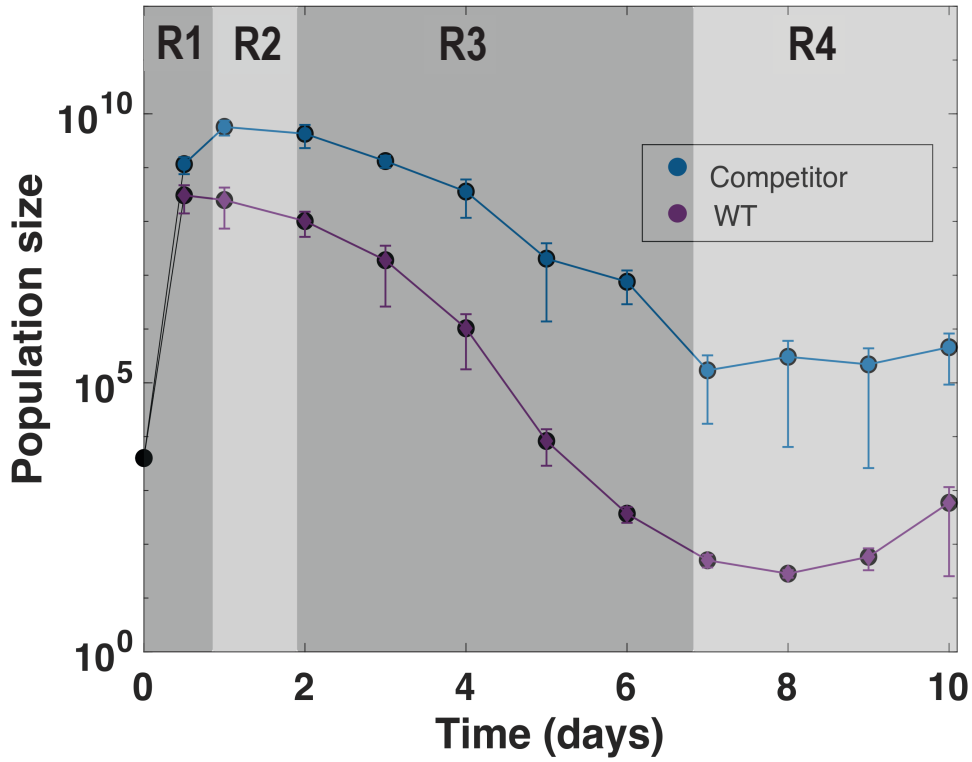

Fig. S11: Different regimes used for mathematical modelling. PA-*S*.Tm-vaccinated 129S6/SvEv mice were pretreated with streptomycin and infected with a total of 10^4 of a 1:1 mixture of *S*.Tm^{WT} (blue symbols) and *S*.Tm^{Comp} (purple symbols). R_1 defines the time window where *S*.Tm^{WT}, *S*.Tm^{Comp} and the microbiota are all below their carrying capacity. R_2 is defined by *S*.Tm^{Comp} being more abundant than *S*.Tm^{WT} and the microbiota, and being in the order of magnitude of K_1. R_3 is defined by the microbiota being more abundant than *S*.Tm^{WT} and *S*.Tm^{Comp} but *S*.Tm^{Comp} is still present in higher numbers than its carrying capacity in equilibrium K_2. R_4 is defined by the microbiota being much more abundant than *S*.Tm^{WT} and *S*.Tm^{Comp} and *S*.Tm^{Comp} being in the order of magnitude of K_2.

Case where microbiota private-resources (K_3) $\gg$ resources shared by *Salmonella* and the microbiota (K_1)

Regime R_1 (i.e. rapid expansion phase) with starting population sizes (W, M, C) $\ll K_1$

In this case, the equations become:

$$\begin{cases} \frac{dW}{dt} = W \cdot (r_w - c_w) \\ \frac{dC}{dt} = C \cdot (r_c - c_c) \\ \frac{dM}{dt} = M \cdot (r_m - c_m) \end{cases}$$

Thus, we have

$$\begin{cases} W(t) \sim \exp\left(t \cdot (r_w - c_w)\right) \\ C(t) \sim \exp\left(t \cdot (r_c - c_c)\right) \end{cases}$$

$$M(t) \sim \exp\left(t \cdot (r_m - c_m)\right)$$

Regime R_2 (i.e. prior to microbiome recovery) with W, M $\ll$ C$\sim \Theta(K_1)$

In this case, the equations become

$$\begin{cases} \dfrac{dW}{dt} = W \cdot \left(r_w \cdot \left(1 - \dfrac{C}{K_1} \right) - C_w \right) \\ \dfrac{dC}{dt} = C \cdot \left(r_c \cdot \left(1 - \dfrac{C}{K_1} \right) - C_c \right) \\ \dfrac{dM}{dt} = M \cdot \left(r_m \cdot \left(1 - \dfrac{1}{\frac{K_1}{C} + \frac{K_3}{M}} \right) - C_m \right) \end{cases}$$

Note: in this regime, $\frac{K_3}{M} \gg \frac{K_1}{C}$. Thus, we have

$$\begin{cases} W(t) \sim \exp\left(t \cdot \left(r_w \cdot \dfrac{c_c}{r_c} - c_w \right) \right) \\ C(t) \sim K_1 \cdot \left(1 - \dfrac{c_c}{r_c} \right) \\ M(t) \sim \exp\left(t \cdot (r_m - c_m) \right) \end{cases}$$

Note that we assume C is the first to be close to the carrying capacity K_1. Then, at $t = \tau$, we have $M \sim C$, that is

$$K_1 \cdot \left(1 - \frac{c_c}{r_c} \right) \sim m_0 \cdot \exp\left(t \cdot (r_m - c_m) \right)$$

Regime R_3 (i.e. during microbiota regrowth) with C, W $\ll$ M and C $\gg K_2$

In this regime, we have $\frac{K_1}{M+W+C} + \frac{K_2}{C} \sim \frac{K_1}{M} + \frac{K_2}{C} \ll 1$. This implies that there are no nutrients available to C and W. In this case, the equations become

$$\begin{cases} \dfrac{dW}{dt} = W \cdot (-c_w) \\ \dfrac{dC}{dt} = C \cdot (-c_c) \\ \dfrac{dM}{dt} = M \cdot \left(r_m \cdot \left(1 - \dfrac{M}{K_3}\right) - c_m\right) \end{cases}$$

Thus, we have

$$\begin{cases} W(t) \sim \exp\left(-t \cdot (c_w)\right) \\ C(t) \sim \exp\left(-t \cdot (c_c)\right) \\ M(t) \sim K_3 \cdot \left(1 - \dfrac{c_m}{r_m}\right) \cdot \left(1 + \left(\dfrac{K_3}{m_0} \cdot \left(1 - \dfrac{c_m}{r_m}\right) - 1\right) \cdot \left(\exp\left(t \cdot (r_m - c_m)\right)\right)\right)^{-1} \end{cases}$$

Regime R_4 (i.e. robust microbiome recovery) with W, M $\ll$ C$\sim \Theta(K_2)$

In this case, the equations become

$$\begin{cases} \dfrac{dW}{dt} = W \cdot \left(r_w \cdot (1 - \dfrac{C}{K_2}) - c_w\right) \\ \dfrac{dC}{dt} = C \cdot \left(r_c \cdot (1 - \dfrac{C}{K_2}) - c_c\right) \\ \dfrac{dM}{dt} = M \cdot \left(r_m \cdot (1 - \dfrac{M}{K_3}) - c_m\right) \end{cases}$$

Thus, at long times we have

$$\begin{cases} W(t) \sim \exp\left(t \cdot \left(r_w \cdot \frac{c_c}{r_c} - c_w\right)\right) \\ C(t) \sim K_2 \cdot \left(1 - \frac{c_c}{r_c}\right) \\ M(t) \sim K_3 \cdot \left(1 - \frac{c_m}{r_m}\right) \end{cases}$$

In this regime, the slopes expected for log (C) and log (W) are $-c_c$ and $-c_w$, respectively. Thus, if we estimate the slopes of log (C) and log (W) from *in vivo* data (vaccinated group) for R_3, we should get an estimation of the clearance rate values. Table S4 shows the slopes obtained from experiments: they range from -1.8 to -3.9 day^{-1}, which would correspond to extremely slow clearance rates. This suggests that the case $K_1 \gg K_3$ is probably not well suited to describe the data.

Width of the regime	Slope for log (C)	Slope for log (W)
day 3 to day 7	-3.4 day^{-1}	-2.2 day^{-1}
day 3 to day 6	-3.7 day^{-1}	-1.8 day^{-1}
day 4 to day 7	-3.3 day^{-1}	-2.4 day^{-1}
day 4 to day 6	-3.9 day^{-1}	-1.9 day^{-1}

Table S4: Estimation of the slopes of log (C) and log (W) from *in vivo* data (vaccinated group + *S*.Tm^{Comp}). The estimation was performed for different possible durations of this regime.

Case where shared resources (K_1) ≫ microbiota-specific resources (K_3)

Regime R_1 with W, M, C $\ll K_1$

If we also have M $\ll K_3$, the equations become

$$\begin{cases} \frac{dW}{dt} = W \cdot (r_w - c_w) \\ \frac{dC}{dt} = C \cdot (r_c - c_c) \\ \frac{dM}{dt} = M \cdot (r_m - c_m) \end{cases}$$

Thus, we have

$$\begin{cases} W(t) \sim \exp\left(t \cdot (r_w - c_w)\right) \\ C(t) \sim \exp\left(t \cdot (r_c - c_c)\right) \\ M(t) \sim \exp\left(t \cdot (r_m - c_m)\right) \end{cases}$$

Regime R_2 with W, M $\ll$ C$\sim \Theta(K_1)$

In this case, the equations become

$$\begin{cases} \dfrac{dW}{dt} = W \cdot \left(r_w \cdot \left(1 - \dfrac{1}{\dfrac{K_1}{C}} \right) - C_w \right) \\ \dfrac{dC}{dt} = C \cdot \left(r_c \cdot \left(1 - \dfrac{1}{\dfrac{K_1}{C}} \right) - C_c \right) \\ \dfrac{dM}{dt} = M \cdot \left(r_m \cdot \left(1 - \dfrac{1}{\dfrac{K_1}{C} + \dfrac{K_3}{M}} \right) - C_m \right) \end{cases}$$

Thus, we have

$$\begin{cases} W(t) \sim \exp\left(t \cdot \left(r_w \cdot \dfrac{c_c}{r_c} - c_w \right) \right) \\ C(t) \sim K_1 \cdot \left(1 - \dfrac{c_c}{r_c} \right) \end{cases}$$

When M is in a regime such that $K_3 \ll M \ll K_1$, then $M(t) \sim \exp\left(t \cdot \left(r_m \cdot \frac{c_c}{r_c} - c_m \right) \right)$.

Regime R_3 with C, W ≪ M and C ≫ K_2

In this case, the equations become

$$\begin{cases} \dfrac{dW}{dt} = W \cdot \left(r_w \cdot \left(1 - \dfrac{M}{K_1} \right) - c_w \right) \\ \dfrac{dC}{dt} = C \cdot \left(r_c \cdot \left(1 - \dfrac{M}{K_1} \right) - c_c \right) \\ \dfrac{dM}{dt} = M \cdot \left(r_m \cdot \left(1 - \dfrac{M}{K_1} \right) - c_m \right) \end{cases}$$

Thus, we have

$$\begin{cases} W(t) \sim \exp\left(t \cdot \left(r_w \cdot \dfrac{c_m}{r_m} - c_w \right) \right) \\ C(t) \sim \exp\left(t \cdot \left(r_c \cdot \dfrac{c_m}{r_m} - c_c \right) \right) \\ M(t) \sim (K_1) \cdot \left(1 - \dfrac{c_m}{r_m} \right) \end{cases}$$

Regime R_4 with W, M $\ll$ C$\sim \Theta(K_2)$

In this case, the equations become

$$\begin{cases} \dfrac{dW}{dt} = W \cdot \left(r_w \cdot \left(1 - \dfrac{1}{\frac{K_1}{M} + \frac{K_2}{C}} \right) - c_w \right) \\ \dfrac{dC}{dt} = C \cdot \left(r_c \cdot \left(1 - \dfrac{1}{\frac{K_1}{M} + \frac{K_2}{C}} \right) - c_c \right) \\ \dfrac{dM}{dt} = M \cdot \left(r_m \cdot \left(1 - \dfrac{M}{K_1} \right) - c_m \right) \end{cases}$$

Thus, we have

$$\begin{cases} W(t) \sim \exp\left(t \cdot \left(r_w \cdot \dfrac{c_c}{r_c} - c_w \right) \right) \\ C(t) \sim \dfrac{K_2}{\left(\frac{1}{1 - \frac{c_c}{r_c}} \right) - \left(\frac{1}{1 - \frac{c_m}{r_m}} \right)} \\ M(t) \sim (K_1) \cdot \left(1 - \dfrac{c_m}{r_m} \right) \end{cases}$$

Kinetic parameter estimation

Below we describe the different methods use to estimate the values of the kinetic parameters of the model from the competition data (see fig. S10). Table 1 recapitulates these results. These results suggest that *S*.Tm^{Comp} has a higher replication rate than the *S*.Tm^{WT} and that vaccination induces a higher clearance rate for *S*.Tm^{WT} strain.

Replication rates

The replication rates can be estimated from in vivo experiments using *Salmonella* carrying a low-copy-number plasmid with an IPTG-dependent origin of replication (pAM34) (*11*) (see fig. S10 A and B). pAM34 carriage can be tracked by ampicillin resistance encoded on the plasmid, on IPTG-containing agar. In the absence of IPTG, the plasmid fails to replicate and after a brief dilution phase, half of the daughter cells and each division will be plasmid-negative and therefore ampicillin-sensitive. Therefore, the final proportions of plasmid-carriers y_0 can be linked to the number of generations, g_0:

$$\log 2(y_0) = d - (1 - \varepsilon) \cdot g_0$$

where 2^d and ε are related to the initial number of plasmid copies per cell and to the residual replication rate of the plasmid, respectively. The measurement of the *in vitro* proportion of plasmid-carriers y_0 for successive dilutions enables the estimation of *d* and ε. Table S5 shows the estimation of *d* and ε values from *in vitro* data.

Strain	*d*	ε
S.Tm^{WT} Kan^{R}	2.15	0.11
S.Tm^{WT} Cm^{R}	1.9	0.1
S.Tm^{Comp} Cm^{R} (D0)	3.43	0.22
S.Tm^{Comp} Cm^{R} (D-3)	3.38	0.16

Table S5: Estimation of *d* and ε from *in vitro* data. The value in brackets for *S*.Tm^{Comp} gives the day when *S*.Tm^{Comp} was given as compared to *S*.Tm^{WT}.

The replication rates can then be obtained from *in vivo* competition data. Indeed, in these experiments, each strain followed an exponential growth regime at short times. In this regime, we can estimate the number of generations *g* at time *t* given access to the maximum replication rate *r* as

$$2^g = \exp(r \cdot t)$$

Here *g* was estimated from the *in vivo* proportion of plasmid-carriers at 12 h post infection and from the *in vitro* estimation of *d* and ε. Table S6 shows the growth rate calculated for each strain for the different competition conditions.

Group	Strain	Growth rate (day^{-1})	# mice
Naive w/o *S*.Tm^{Comp}	*S*.Tm^{WT} Kan^{R}	34.4±2.4	3
	S.Tm^{WT} Cm^{R}	32±3.3	2
Naive + *S*.Tm^{Comp}	*S*.Tm^{WT} Kan^{R}	31.8±4.8	3
	S.Tm^{Comp} Cm^{R}	36±4.3	3
Vacc. w/o *S*.Tm^{Comp}	*S*.Tm^{WT} Kan^{R}	30.4	1
	S.Tm^{WT} Cm^{R}	25.9±3.6	2

Vacc. + *S*.Tm^{Comp}	*S*.Tm^{WT} Kan^{R}	33.7±3.7	3
	S.Tm^{Comp} Cm^{R}	38.7±0.4	3

Table S6: Estimation of the growth and clearance rates from *in vivo* competition data at *t* = 12 h. For each experiment *k*, we have expressed the value of the growth rate r_k as $r_k = \overline{r_k} \pm \delta r_k$ with $\overline{r_k} = \frac{1}{n} \cdot \sum_{i=1}^{n} r_{i,k}$ and $\delta r_k = \frac{1}{n-1} \cdot \sum_{i=1}^{n} \left(r_{i,k} - \overline{r_k}\right)^2$. The index *n* (column #) corresponds to the number of mice having not out-diluted plasmids at *t* = 12 h. Initial *S*.Tm^{WT} Kan^{R}/*S*.Tm^{WT} Cm^{R} CFU: 6000-7500. Initial *S*.Tm^{WT} Kan^{R}/*S*.Tm^{Comp} Cm^{R} CFU: 3600.

Clearance rates, c

To estimate the clearance rates in naive mice, we have used the fact that the size of *S*.Tm^{WT} starts to decrease exponentially after a few days in the presence of the competitor strain. For the naive group, we can thus write

$$W_{naive}(t) \sim \exp\left(\left(r_w \cdot \frac{c_c}{r_c} - c_{w,naive}\right) \cdot t\right)$$

that is

$$\log\left(W_{naive}(t)\right) = \Delta r_n \cdot t + \gamma = \left(r_w \cdot \frac{c_c}{r_c} - c_{w,naive}\right) \cdot t + \gamma$$

This holds approximatively from day 1 to day 8 post infection, after which the bacterial number plateaus. Here we suppose that the clearance rates of *S*.Tm^{WT} and *S*.Tm^{Comp} are similar in the naïve case, that is $c_{w,naïve} = c_c$. The underlying hypothesis is that the clearance rates of *S*.Tm^{WT} and *S*.Tm^{Comp} are only different in the vaccinated group due to more efficient clearance of aggregated *S*.Tm^{WT} (*7, 9*). Thus, the slope $\Delta r_n \left(r_w \cdot \frac{c_c}{r_c} - c_c\right)$ can be estimated from the *in vivo* CFUs. If we use the replication rates estimated above and make the assumption that the clearance rate of *S*.Tm^{Comp} and *S*.Tm^{WT} are the same in the naive case, we get the naïve clearance rate as

$$c_c = \Delta r_n \cdot \left(\frac{r_w}{r_c} - 1\right)^{-1}$$

Similarly for the vaccinated group from day 1 to day 3 post infection, we can write

$$W_{vacc}(t) \sim \exp\left(\left(r_w \cdot \frac{c_c}{r_c} - c_{w,vacc}\right) \cdot t\right)$$

1119 that is

$$\log\left(W_{vacc}(t)\right) = \Delta r_v \cdot t + \delta = \left(r_w \cdot \frac{c_c}{r_c} - c_c\right) \cdot t + \delta$$

1120 Again Δr_v can be estimated from the data and using the value of c_c obtained from the naive case, we
1121 get an estimation for the clearance rate of *S*.Tm^{WT} in the vaccinated case:

$$c_w = r_w \cdot \frac{c_c}{r_c} - \Delta r_v$$

1122 Table S7 shows the values of c_w and c_c estimated with this method.

1123

r_w (day^{-1})	r_c (day^{-1})	c_w (day^{-1})	c_c (day^{-1})
33.7	38.7	6.4	5.9

1124 **Table S7:** Clearance rate values.

1125 *Carrying capacities, K*

1126 Three carrying capacities need to be estimated. K1 can be obtained from the following expression:

$$K_1 \sim C_{max} \cdot \left(1 - \frac{c_c}{r_c}\right)^{-1}$$

1127 where C_{max} is the size of the *S*.Tm^{Comp} population at its maximum (typically at *t* = 24 h) in the vaccinated
1128 group.

1129

1130 For K_2, we have

$$K_2 \sim C_{plateau} \cdot \left(\left(\frac{1}{1 - \frac{c_c}{r_c}}\right) - \left(\frac{1}{1 - \frac{c_m}{r_m}}\right)\right)$$

where $C_{plateau}$ is the mean size of the *S*.Tm^{Comp} population when it reaches a plateau around 7-10 days post infection. This estimation leads to $K_1 = 5.9 \cdot 10^9$ and $K_2 = 2.3 \cdot 10^4$. The value of K_3 needs to be determined by curve fitting (see below).

Microbiota kinetic parameters: ratio between clearance and replication rate

The ratio between clearance and replication rate can be estimated as follows:

In the case $K_3 \ll K_1$ when the microbiota has recovered (that is $M \gg C,W$) and where $C \gg K_2$, we have

$$\begin{cases} W(t) \sim \exp\left(t \cdot \left(r_w \cdot \frac{c_m}{r_m} - c_w\right)\right) \\ C(t) \sim \exp\left(t \cdot \left(r_c \cdot \frac{c_m}{r_m} - c_c\right)\right) \\ M(t) \sim K_1 \cdot \left(1 - \frac{c_m}{r_m}\right) \end{cases}$$

where r_m and c_m are the replication rate and the clearance rate of the microbiota, respectively.

We thus have

$$\log(C) = \alpha_c \cdot t + \gamma = \left(r_c \cdot \frac{c_m}{r_m} - c_c\right) \cdot t + \gamma$$

$$\log(W) = \alpha_w \cdot t + \gamma = \left(r_w \cdot \frac{c_m}{r_m} - c_w\right) \cdot t + \gamma$$

where the value of the slopes α_c and α_w can be estimated experimentally and gives access to the ratio between clearance and replication rate of the microbiota, $\frac{c_m}{r_m}$. The ratio was calculated as

$$\frac{c_m}{r_m} = 0.5 \cdot \left((\alpha_c + c_c) \cdot \left(\frac{1}{r_c}\right) + (\alpha_w + c_w) \cdot \left(\frac{1}{r_w}\right)\right)$$

Data fitting

Three kinetic parameter values still need to be estimated: the size of the microbiota at *S*.Tm infection, m_0, the microbiota replication, r_m (its clearance rate is then directly obtained from the ratio estimated above) and the value of the carrying capacity K_3.

These parameters were estimated by fitting the model to the *S*.Tm^{WT} and *S*.Tm^{Comp} data (vaccinated group) with a least squares method (see Fig. S12A for the best fit and table S8 for the corresponding values).

m_0 (CFUs g^{-1} feces)	r_m (day^{-1})	K_3	Res. norm
10^5	18.7	10^7	4

Table S8: Parameter values obtained from data fitting. The fit was performed with the nonlinear least-squares solver lsqcurvefit of MATLAB R2015a. corresponds to the value of the squared 2-norm of the residual $\sum(f(\rho, xdata) - \log_{10}(ydata))^2$ with p = r_m and where f is the $\log_{10}$ of the solution of the ODE system. The algorithm was run for m_0 values ranging between 10^5 and 10^7. The algorithm was run for K_3 values ranging between 10^7 and $5 \cdot 10^8$.

Extinction probability and extinction time: critical parameters for protection

For an intervention (either vaccination, or niche competition, or both combined) to be beneficial, it must minimize the time needed for the extinction of the *S*.Tm^{WT} population. For the sake of simplicity, we only consider cases where the initial number of newly introduced bacteria is large, that is $W_0 > 100$. In this case, the dynamics of the invasion process can be divided into two time windows (Fig. S12). The first time window starts with the inoculation and ends when the number of *S*.Tm^{WT} bacteria becomes < 100: all populations are thus large so that time spent in this time window is evaluated by integrating until the time τ when W (τ) = 100 for the following deterministic equations:

$$\begin{cases} \frac{dW}{dt} = W \cdot \left(r_w \cdot \left(1 - \frac{1}{\frac{K_1}{M+C+W} + \frac{K_2}{C+W}} \right) - c_w \right) \\ \frac{dC}{dt} = C \cdot \left(r_c \cdot \left(1 - \frac{1}{\frac{K_1}{M+C+W} + \frac{K_2}{C+W}} \right) - c_c \right) \\ \frac{dM}{dt} = M \cdot \left(r_m \cdot \left(1 - \frac{1}{\frac{K_1}{M+C+W} + \frac{K_3}{M}} \right) - c_m \right) \end{cases}$$

The second time window starts when the resident population becomes < 100 and ends with its extinction: a stochastic description is used here because of the small size of the resident population. The distribution of the times needed to go from W = 100 to extinction can be obtained numerically with the Gillespie algorithm.

Using 2500 iterations of a stochastic version of this model, we could derive extinction-related parameters. Based on continuous growth and clearance of the gut luminal *Salmonella* population, these models indicate clearance of virulent *Salmonella* within eight days of infection in mice treated with the vaccine-enhanced competition regimen (i.e. vaccination plus *S*.Tm^{Comp}), compared to continuous colonization in untreated or vaccine-only mice (Fig. M3). Note that while microbiota re-growth can be a major contributor to K_1 in vaccinated mice, in the absence of competitor we still expect the entirety of K_2 to be made up of *S*.Tm^{WT}, i.e. we never see complete clearance. As the relative size of K_1, K_2 and K_3 will vary based on the microbiome composition, the host diet, and any perturbations applied to the system such as antibiotics or diet shifts, the relative importance of the competitor will also vary in real-world situations. The model therefore predicts that both vaccination and niche competition as required to drive pathogen extinction, and that clearance is expected between 6 and 12 days post-exposure.

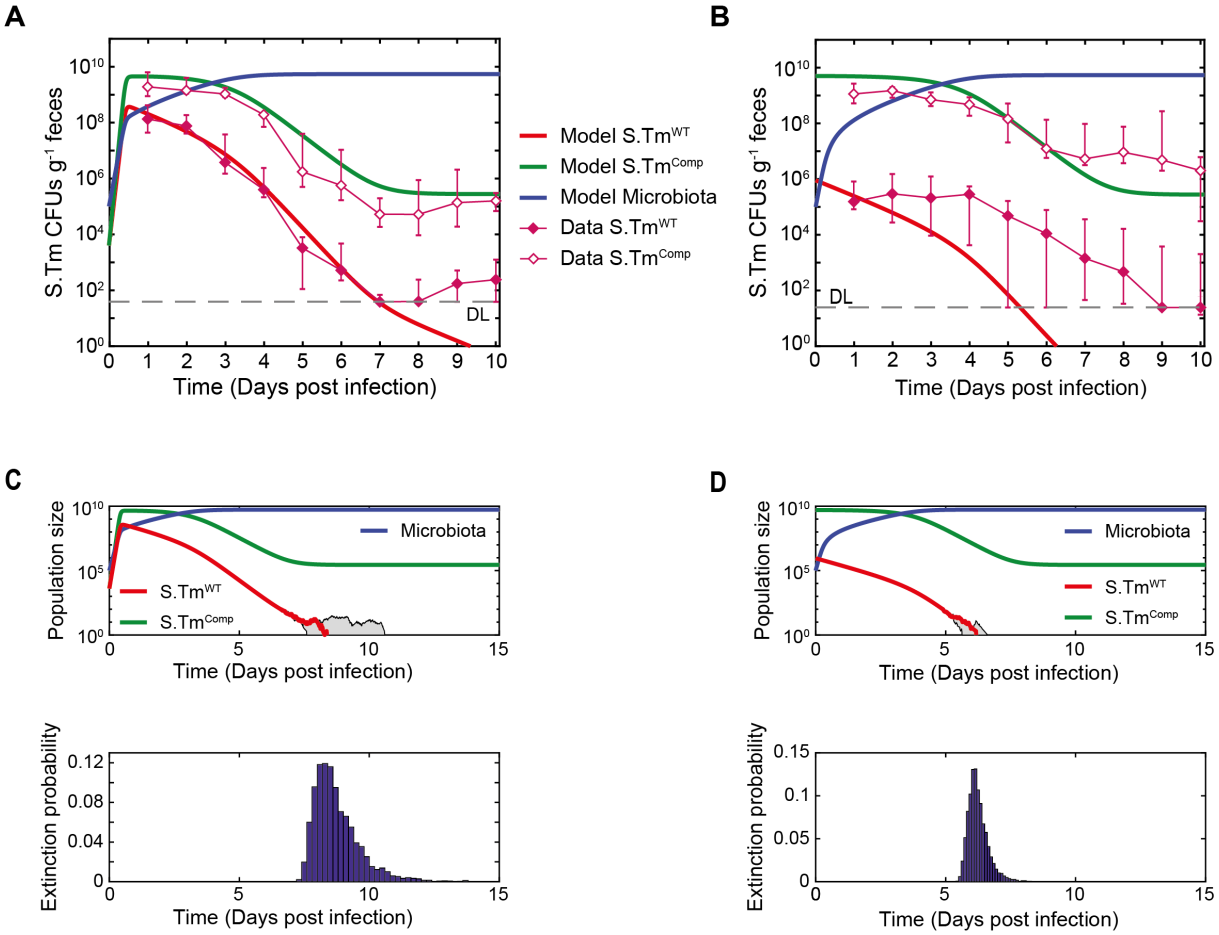

Fig. S12: Modelling of *S*.Tm^{WT} extinciton for simultaneous or a priori *S*.Tm^{Comp} colonization, in vaccinated mice. (**A**) The model was adjusted to experimental data where *S*.Tm^{Comp} was administered simultaneous to infection. The thick lines correspond to the best fit from the model and the thin lines with diamonds to the experimental data (median ± interquartile range). Initial *S*.Tm^{WT} and *S*.Tm^{Comp} CFUs: $4{\cdot}10^3$. (**B**) Comparison of the predictions of the model to data where *S*.Tm^{Comp} was administered 3 days before infection, in vaccinated mice. The thick solid lines correspond to the prediction from the model, using the value of the dynamical parameter inferred from an experiment with simultaneous *S*.Tm^{WT} and *S*.Tm^{Comp} infection. The thin lines with diamonds to the experimental data (median ± interquartile range). Initial *S*.Tm^{WT} CFUs: $9{\cdot}10^5$. Initial *S*.Tm^{Comp} CFUs: $4{\cdot}10^3$. Parameter values: $r_w = 33.7$ day^{-1}, $c_w = 6.4$ day^{-1}, $r_c = 38.7$ day^{-1}, $c_c = 5.9$ day^{-1}, $r_m = 18.7$ day^{-1}, $c_m = 1.7$ day^{-1}, $K_1 = 5.9{\cdot}10^9$, $K_2 = 2.3{\cdot}10^4$, $K_3 = 10^7$ and $m_0 = 10^5$. r_w, r_c and r_m: growth rate of *S*.Tm^{WT}, *S*.Tm^{Comp} and the microbiota, respectively. c_w, c_c and c_m: clearance rates of *S*.Tm^{WT}, *S*.Tm^{Comp} and the microbiota. K_1, K_2, K_3: carrying capacities of *S*.Tm and the microbiota, *S*.Tm^{WT} and *S*.Tm^{Comp} and the microbiota alone. m_0: size of microbiota after antibiotic clearance. For parameter estimation, our computations were based on the log of the arithmetic mean of experimental data (4 mice). (**C**) Extinction time probability distribution for *S*.Tm^{WT} and *S*.Tm^{Comp} given simultaneously. Simulations were performed with the deterministic model for large population size. For small size of *S*.Tm^{WT} population (*S*.Tm^{WT} < 100), simulations were performed with the Gillespie algorithm (5000 realizations). Upper panel: the red line corresponds to a trajectory whose extinction time is around the median extinction time. The gray area shows trajectories of the 2.5th percentile extinction time and the 97.5th percentile extinction time. Lower panel: extinction time probability distribution. The y-axis corresponds to (bin height*bin width). Median extinction time: 8.5 days. 2.5th percentile: 7.6 days. 97.5th percentile: 11 days. Initial *S*.Tm^{WT} CFUs: $4{\cdot}10^3$. Initial *S*.Tm^{Comp} CFUs: $4{\cdot}10^3$. (**D**) Extinction time probability distribution for a priori colonization with *S*.Tm^{Comp}. Simulations were performed with the deterministic model for large population size. For small size of *S*.Tm^{WT} population (*S*.Tm^{WT} < 100), simulations were performed with the Gillespie algorithm (5000 realizations). Upper panel: the red line corresponds to a trajectory whose extinction time is around the

median extinction time. The gray area shows trajectories of the 2.5th percentile extinction time and the 97.5th percentile extinction time. Lower panel: extinction time probability distribution. The y-axis corresponds to (bin height*bin width). Median extinction time: 6 days. 2.5th percentile: 5.7 days. 97.5th percentile: 7.2 days. Initial *S*.Tm^{WT} CFUs: $9 \cdot 10^5$. Initial *S*.Tm^{Comp} CFUs: $4 \cdot 10^3$. The dotted line depicts the mean detection limit of the experimental data. (A, C+D) Parameter values: $r_w = 33.7\ day^{-1}$, $c_w = 6.4\ da^{-1}$, $r_c = 38.7\ day^{-1}$, $c_c = 5.9\ day^{-1}$, $r_m = 18.7\ day^{-1}$, $c_m = 1.7\ day^{-1}$, $K_1 = 5.9 \cdot 10^9$, $K_2 = 2.3 \cdot 10^4$, $K_3 = 10^7$ and $m_0 = 10^5$. r_w, r_c and r_m: growth rate of *S*.Tm^{WT}, *S*.Tm^{Comp} and the microbiota, respectively. c_w, c_c and c_m: clearance rates of *S*.Tm^{WT}, *S*.Tm^{Comp} and the microbiota. K_1, K_2, K_3: carrying capacities of *S*.Tm and the microbiota, *S*.Tm^{WT} and *S*.Tm^{Comp} and the microbiota alone. m_0: size of microbiota after antibiotic clearance.

Supplementary References

45. A. J. Grant *et al.*, Modelling within-host spatiotemporal dynamics of invasive bacterial disease. *PLoS Biol* **6**, e74 (2008).
46. B. Stecher *et al.*, Gut inflammation can boost horizontal gene transfer between pathogenic and commensal Enterobacteriaceae. *Proc Natl Acad Sci U S A* **109**, 1269-1274 (2012).
47. A. Rasko David *et al.*, The Pangenome Structure of Escherichia coli: Comparative Genomic Analysis of E. coli Commensal and Pathogenic Isolates. *Journal of Bacteriology* **190**, 6881-6893 (2008).
48. S. Hapfelmeier *et al.*, The Salmonella pathogenicity island (SPI)-2 and SPI-1 type III secretion systems allow Salmonella serovar typhimurium to trigger colitis via MyD88-dependent and MyD88-independent mechanisms. *J Immunol* **174**, 1675-1685 (2005).
49. L. M. Guzman, D. Belin, M. J. Carson, J. Beckwith, Tight regulation, modulation, and high-level expression by vectors containing the arabinose PBAD promoter. *J Bacteriol* **177**, 4121-4130 (1995).
50. P. P. Cherepanov, W. Wackernagel, Gene disruption in Escherichia coli: TcR and KmR cassettes with the option of Flp-catalyzed excision of the antibiotic-resistance determinant. *Gene* **158**, 9-14 (1995).
51. Y. Zhang *et al.*, Multicopy Chromosomal Integration Using CRISPR-Associated Transposases. *ACS Synth Biol* **9**, 1998-2008 (2020).
52. G. J. McKenzie, N. L. Craig, Fast, easy and efficient: site-specific insertion of transgenes into Enterobacterial chromosomes using Tn7 without need for selection of the insertion event. *BMC microbiology* **6**, 39 (2006).
53. K. A. Datsenko, B. L. Wanner, One-step inactivation of chromosomal genes in Escherichia coli K-12 using PCR products. *Proc Natl Acad Sci U S A* **97**, 6640-6645 (2000).
54. N. L. Sternberg, R. Maurer, Bacteriophage-mediated generalized transduction in Escherichia coli and Salmonella typhimurium. *Methods Enzymol* **204**, 18-43 (1991).
55. M. Sobota *et al.*, The expression of virulence genes increases membrane permeability and sensitivity to envelope stress in Salmonella Typhimurium. *PLOS Biology* **20**, e3001608 (2022).
56. E. Bakkeren *et al.*, Impact of horizontal gene transfer on emergence and stability of cooperative virulence in Salmonella Typhimurium. *Nat Commun* **13**, 1939 (2022).
57. K. Moor *et al.*, Analysis of bacterial-surface-specific antibodies in body fluids using bacterial flow cytometry. *Nat Protoc* **11**, 1531-1553 (2016).